Graphical Abstract

Modelling of thin constrained layer damping treatment applied to composite floor beams

Carlos M. C. Renedo, Iván M. Díaz, Jaime H. García-Palacios

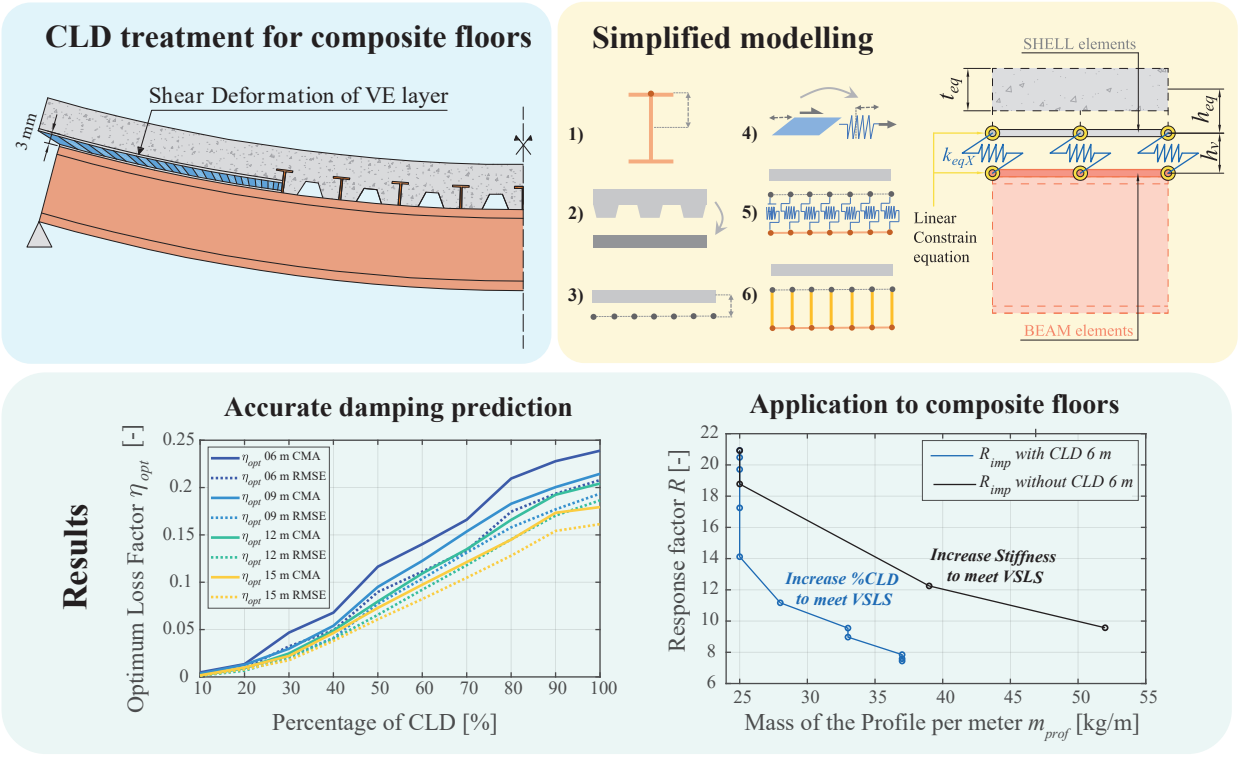

Highlights

Modelling of thin constrained layer damping treatment applied to composite floor beams

Carlos M. C. Renedo, Iván M. Díaz, Jaime H. García-Palacios

- A modelling approach based on a simplified finite element model and the use of a corrected modal strain energy method has been proposed to model viscoelastic constrained layer damping treatments applied to composite floors, for them to meet vibration serviceability criteria.
- A parametric study has been carried out varying the viscoelastic treatment, the length of the beam and the stiffness of the Viscoelastic core.
- The simplified approach predicts accurately the resulting modal damping ratios as compared to the most detailed modelling approaches.
- The proposed approach is clearly geared to engineering practice due to its simplicity when designing lighter composite floors with viscoelastic treatments. The approach is adequate to perform structural optimization of this kind of floor.

Modelling of thin constrained layer damping treatment applied to composite floor beams

Carlos M. C. Renedo[a], Iván M. Díaz[a], Jaime H. García-Palacios[b]

[a]*Department of Continuum Mechanics and Theory of Structures, ETSI Caminos, Canales y Puertos, Universidad Politécnica de Madrid, Calle Profesor Aranguren 3, Madrid, 28040, Comunidad de Madrid, Spain*
[b]*Department of Hydraulics, Energy and Environmental Engineering, ETSI Caminos, Canales y Puertos, Universidad Politécnica de Madrid, Calle Profesor Aranguren 3, Madrid, 28040, Comunidad de Madrid, Spain*

Abstract

The Vibration Serviceability Limit State (VSLS) due to human dynamic loading is increasingly becoming the sizing criterion for long-span composite floors. To meet this requirement, structural designers usually tend to increase the stiffness or the mass of the floor. This paper studies a damping technology applicable to these floors since the design stage for improving their dynamic behaviour by increasing their damping capacity and avoiding thus over-sizing the floor structure to meet the VSLS. The studied technology is based on a Constrained Layer Damping (CLD) treatment made of a thin viscoelastic (VE) layer integrated between the concrete slab and the steel profile of the floor, along a percentage of the beam length near the supports. Thus, this paper proposes a simplified Finite Element (FE) approach to model this treatment based on using simple SPRING elements for the VE layer and a corrected version of the modal strain energy method for damping estimation, avoiding thus the use of complex modal analysis. The proposed approach is used to assess the additional damping ratio provided by the CLD treatment. The accuracy of this approach has been validated by comparing it with detailed FE models

Preprint submitted to Structures

and widely accepted analytical formulations considering different percentages of the beams' length treated with CLD. Finally, an application example has been performed with CLD-treated and untreated single-spanning composite floors, showing: i) CLD-treated floors have a better dynamic performance, and ii) CLD technology enables reducing the amount of steel needed to design lightweight floors especially sensitive to vibration.

Keywords: Vibration Serviceability, Floor Vibrations, Constrained Layer Damping, Viscoelastic Damping.

---

1. Introduction

Currently, due to architectural and cost constraints, there is an increased demand for slender and longer-span floor systems realized with lighter structures that offer more sustainable solutions [1]. The increasing use of open-plan offices has led to a reduction of dead and live loads due to the removal of full-height partitions and heavy furnishing elements (1 kPa less) [2], [3]. This scenario has contributed to developing composite floors with lower natural frequencies (lower than 10 Hz) and with lower inherent damping ratios (2.5 % or even less once occupied). As a consequence, many composite floors show excessive vibrations due to human-induced dynamic loading [4]. Additionally, as vibration comfort levels required for floor systems are quite restrictive (0.02-0.05 m/s^2 for offices [5]) the Vibration Serviceability Limit State (VSLS) has become an important governing factor to consider when designing long-span composite floor systems [6].

Low-Frequency Floors (LFFs, those with fundamental natural frequencies lower than 10 Hz) tend to exhibit resonant dynamic responses produced by the higher harmonics (3^{rd} or 4^{th}) of the human-induced loading [7]. Knowing this, structural

designers usually tend to first, design High-Frequency floors (HFFs) by including stiffer-enough steel members in the composite design. A second strategy to face VSLS problems at the design stage may be the use of heavy concrete slabs that increase the structural mass, proportionally decreasing the vibration amplitude at resonance [8]. Both approaches directly affect the lightness of the floor increasing its embodied carbon [9]. Thirdly, the integration of damping strategies can be an effective way to reduce vibrations in LFFs [10]. This latter may also contribute to reducing the use of structural material to overcome these problems, thus, reducing the building's embodied carbon footprint. This is a key point considering that floors are responsible for more than 40% of the total embodied carbon of the structure of a building [11].

Regarding damping strategies applied to solve floor vibrations, there are two main alternatives. First, the use of inertial dampers, in their passive (the so-called Tuned Mass Dampers or TMDs [12]), semi-active [13] and active versions [14], that apply counteract forces to reduce the structural motion. They usually suffer from detuning problems and are difficult to integrate into the floor design [15]. Active versions are effective, but energy consumption during their life cycle should be considered. The second alternative consists in increasing the inherent damping of the structure through the integration of viscoelastic (VE) materials at specific locations where they can dissipate additional energy. An effective way of doing so is through using Constrained Layer Damping (CLD) treatments, where a thin VE layer is embedded between two elastic bending members creating a sort of *"sandwich beam"*. When this beam vibrates in bending modes the VE core greatly deforms to shear achieving the intended energy dissipation through a stress-strain shear hysteresis [16].

CLD treatments have been extensively used in aerospace and mechanical structures to reduce broad-band frequency vibrations [17], however, their use in civil

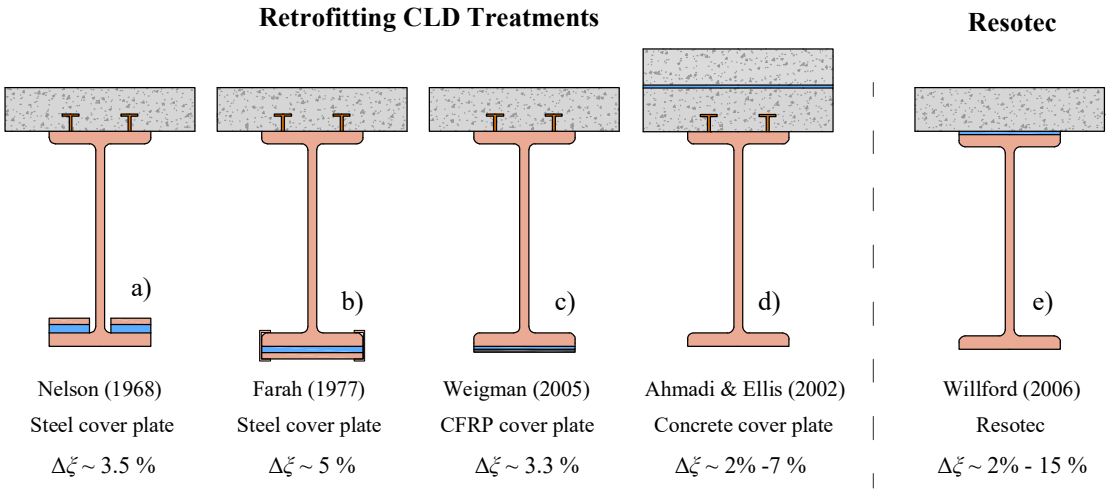

Figure 1 Evolution in the application of CLD treatments to composite floor systems

Figure 1: Evolution in the application of CLD treatments to composite floors.

engineering structures is still limited [18], [19]. The initial applications of CLD treatments to composite floors to increase their damping ratio were developed as retrofitting solutions (Figures 1a, [20], and 1b, [21]) achieving damping ratio increases of 3.5% to 5%. Later, investigations were conducted by Ebrahimpour and Ahmadi et al. obtaining similar results, but with different CLD configurations (Figures 1c, [22] and 1d, [23]). In 2006 ARUP in collaboration with Richard Lee Steel Decking proposed the first commercial CLD solution to be integrated into a composite floor since the construction stage. This was called "Resotec" (Figure 1e), and its applicability was described by Willford et al. [24]. The system was conceived to be applied to the secondary beams of a composite floor as depicted in Figure 2. The major advance of this proposal over the previous ones was to locate the VE layer between the rib deck concrete slab and the upper flange of the steel beam (as close as possible to the composite section centroid) where the shear strain is maximum. Besides, they recommended including the VE layer only for a percentage of the beam's

length near the supports, where the longitudinal shear strain is higher, whereas the central part of the composite beam remains connected to shear by means of studs. Therefore, there is a trade-off between the achieved inherent damping and the loss of stiffness due to the partial shear connection in length. The CLD treatment itself used by ARUP has an overall thickness of 3mm and is composed of two thin steel sheets of 1mm that constrain a slim VE layer of 1mm. The present paper is focused on studying CLD treatments similar to the one proposed by Willford et al.

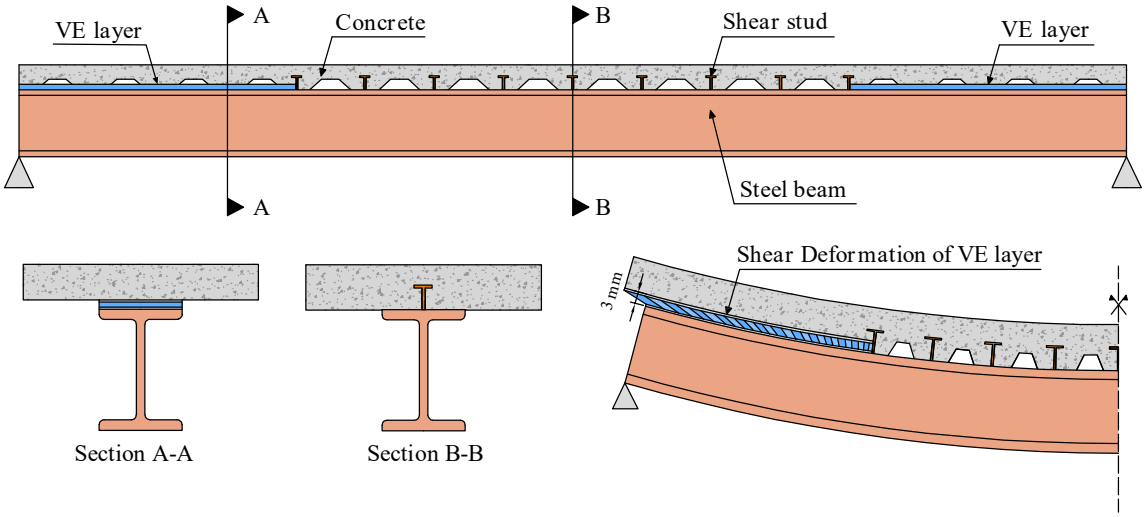

Figure 2 *"Resotec"* CLD treatment installed along the 50% of the beam length (50% CLD beam, Willford 2006)

Figure 2: *"Resotec"* CLD treatment installed along 50% of the beam. length (50% CLD) Willford et al. [24].

For CLD treatments to be extensively used in composite floor construction is essential to provide a reliable and manageable way of predicting the additional damping ratio that it provides [25]. Different authors have proposed different modelling strategies. First, a well-known Partial Differential Equation (PDE) model of a three-layer *"sandwich beam"* with a VE core was proposed by DiTaranto [26] based on the work of Ross et al. [27]. This model was solved with Complex Modal Analysis (CMA) by

Rao [28] for beams with different boundary conditions. Other authors as Farah et al. [21] and Zegers [29] have used similar formulations to analyze both, CLD retrofitting solutions and solutions similar to *"Resotec"* in composite floors beams applied along the whole beams' length (here named as 100% CLD treated beams). Willford et al. has provided some results for composite beams partially treated in length (for example, 50% CLD treated beams). He claims to use a similar model to the one provided in [28] (Despite this solution being only applicable for 100% CLD cases) but without providing details on how it was applied or solved for partially treated beams. Secondly, some authors have opted for a detailed Finite Element (FE) modelling where the VE layer is represented with solid elements with VE constitutive behaviour and solved with CMA, [23], [30], however, these approaches are complex and do not encourage engineers to use this technology. In this context, the present paper aims to provide a simplified and practitioner-focused modelling methodology to assess CLD treatments through the use of two important characteristics, i) simple elements such as spring elements for the VE layer, and ii) real modal analysis. Thus, first, the methodology proposed has been validated through rigorous comparison of its results for a 100% CLD benchmark beam with two widely accepted modelling approaches, namely: a detailed FE model of the CLD treatment solved with CMA, and the solution of Rao [28]. Second, the proposed methodology has been also validated to model partially treated beams using a similar comparison with the detailed FE model. For that, a parametric analysis with different beam lengths and $\%CLD$ has been carried out. Thirdly, the results obtained in this parametric analysis have been used to assess the dynamic performance of single-spanning composite floors partially treated with CLD.

The remainder of this paper is organized as follows: Section 2 describes a 100% CLD benchmark composite beam used for the first validation of the paper. Section

3 describes the different types of models and analyses used to assess this benchmark beam and compares the results obtained with each modelling approach studied. Section 4 describes the parametric analysis developed to validate the proposed modelling approach for partially treated beams. Section 5 studies as an example of application, the dynamic performance of single-spanning composite floors made with partially treated beams. Finally, Section 6 provides some conclusions and future works.

2. Benchmark floor beam

2.1. Geometry of the benchmark floor beam

The benchmark example used for comparing the modelling approaches is a simply supported secondary floor beam with a 100% CLD treatment. The beam has a length of 12 m and makes use of a UB 457X191X67 steel profile combined with a rib-deck for the concrete slab ALX1.2 mm of gauge (from Richard Lee Steel Decking). The total height of the concrete slab is 130 mm and its width is 2.30 m. The CLD treatment applied consists of two steel sheets of 1 mm thickness comprising a 1 mm VE layer in the middle. The width of the treatment is the same as the one of the steel profile flange, 191 mm.

2.2. Constitutive model

This paper deals with the dynamic structural analysis of floor beams in serviceability conditions. For that, both concrete and steel are modelled as elastic materials. The steel has been modelled with a Young modulus E_s=210 GPa, a Poisson modulus ν_s=0.3 and a density ρ_s=7850 kg/m^3. The concrete has been defined with the following properties, E_c=30 GPa, ν_c=0.2 and ρ_c=2500 kg/m^3.

The VE material is defined through a frequency-domain VE constitutive model. This formulation is obtained by applying the Laplace Transform to the time-domain

equations of the Boltzmann constitutive model for VE materials [17]. Thus, the VE behaviour is modelled with a complex shear modulus $G_v^*(\omega)$, depending on the circular frequency ω, as follows:

$$G_v^*(\omega) = G_v'(\omega) + G_v''(\omega)\, i, \tag{1}$$

where $i = \sqrt{-1}$ is the imaginary unit, $G_v'(\omega)$ and $G_v''(\omega)$ are the shear storage and shear dissipative modulus, representing the elastic and the viscous contributions to the VE behaviour, respectively. Both of them are also frequency-dependant magnitudes. Equation (1) is usually rewritten as:

$$G_v^*(\omega) = G_v'(\omega)(1 + \eta_v(\omega)i), \tag{2}$$

where $\eta_v(\omega)$ is the loss factor which is a measure of the dissipative capacity of the VE material.

In this paper, the VE material of the CLD is defined through G'_v and η_v. These magnitudes can be considered to be constant along the frequency band of inter-est. The value of η_v has been assumed to be constant and equal to 1, however, the value of G_v' has been varied along the whole set of studies performed in the paper, as it will be explained in later sections. Typical values of G_v' for VE materials used in these kind of CLD treatments are around 0.5 to 2 MPa within the low-frequency band between 3 to 10 Hz [31]. Finally, the Poisson coefficient assumed for this ma-terial ν_v has been set to 0.49 (a typical value for an elastomeric material used for these types of damping applications) [32].

3. Modelling approaches

The term "modelling approach" is used in this paper to define the combination of two elements, i) a type of model and ii) a type of modal analysis performed on the model. 3 types of models and 3 types of analysis are described in this section. All of them will be combined defining 9 different modelling approaches that will be compared between each other. The objective of this comparison is to validate the accuracy of one modelling approach proposed by the authors as a simplified option to be used for the design of composite floors with integrated CLD treatments.

3.1. Types of Models

3.1.1. Model 1: Detailed FE model

This first detailed model has been considered to be the reference for comparison in terms of accuracy, as the geometry has been precisely modelled. The FE modelling presented in this paper has been performed in ANSYS Mechanical APDL.

As has been illustrated in Figure 3a, the concrete slab has been modelled with SOLID185 elements using one element along its thickness. The steel rib-deck used for the slab has been modelled with SHELL181 elements rigidly connected to the concrete slab, node by node. The steel beam is defined using SHELL181 elements and a positive offset equal to half of the flange thickness has been used for the elements of the profile's upper flange. Finally, the CLD treatment has been defined using SHELL181 elements for its thin constraining steel sheets, and SOLID185 elements for the VE layer, using only one element along its thickness. The lower constraining steel sheet of the CLD has not been included in the model as its influence is negligible. Additionally, the upper and lower surfaces of the CLD treatment have been rigidly connected to the concrete slab and the steel beam, respectively.

Three main aspects of this model must be highlighted. First, a constraint linear equation has been defined between the top and bottom nodes of the VE layer at any beam section, so they have the same vertical displacement. Second, the upper constraining layer of the CLD treatment (depicted in green in Figure 3a) should be included, as it allows transferring the shear deformation of the VE layer within the rib-deck valleys where the slab is not directly in contact with the CLD treatment (Figure 3b). Third, the length-to-height aspect ratio (AR) of the SOLID185 elements used to model the VE layer (Figure 3c), and the number of these elements included along its thickness have been analyzed. A sensitivity analysis varying this AR was carried out proving that these parameters do not influence significantly the result obtained. An AR of around 100 was finally used in the model.

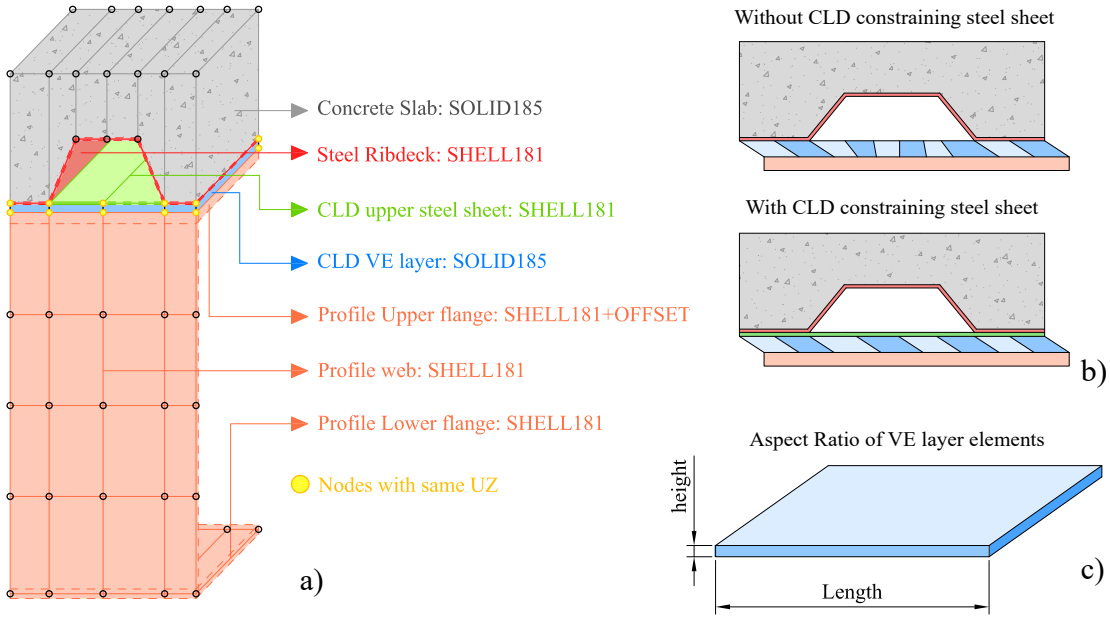

Figure 3: Model 1. Detailed FE model with SOLID185 and SHELL181 elements.

3.1.2. Model 2: Simplified FE model

This second model has been proposed as a simplified approach to modelling the dynamic behaviour of a floor sandwich beam with BEAM, SHELL and SPRING elements. The modelling approach is here described in 4 Steps and is graphically represented in Figure 5:

- *Step 1: Steel profile modelling.*

  The steel profile is modelled with Euler-Bernoulli first-order BEAM elements, particularly, for this paper the authors used BEAM188 from ANSYS. A positive offset equal to half of the profile's height $h_s/2$ is given to the profile's section, so the nodes are located at its top fibre (See Figure 5). A given element length L_{el} is adopted.

- *Step 2: Rib-deck slab modelling.*

  The rib-deck concrete slab is modelled with SHELL elements including nodes just over the nodes of the profile. An equivalent constant-height slab (as the one depicted in Figure 4), which can be defined with four parameters, has been used.

  The equivalent parameters of the slab are obtained as follows [33]. First, the Young Modulus is considered to be equal to the concrete one, E_c. Second, by considering that the bending stiffness of both the real and the equivalent slab must be equal when simply-supported and subjected to a constant bending moment state, the equivalent height, t_{eq}, is computed as follows:

$$t_{eq} = \sqrt[3]{\frac{12(a+b)}{\left(\frac{a}{I_{hA}} + \frac{b}{I_{hB}}\right)}}, \tag{3}$$

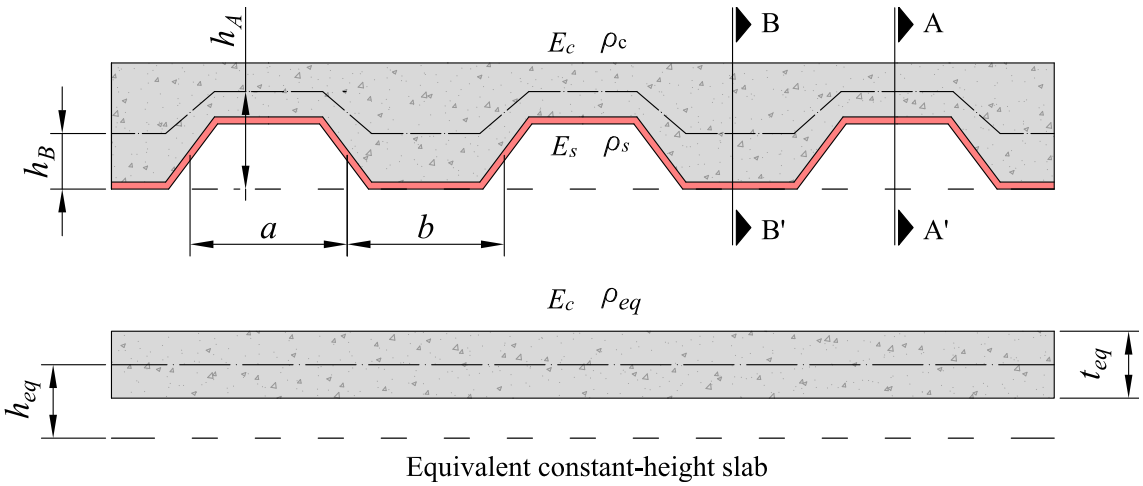

Figure 4: Equivalent constant-thickness concrete slab used in Model 2.

where a and b are the distances depicted in Figure 4, and I_{hA} and I_{hB} are the moments of inertia of the concrete-homogenised sections A-A' and B-B' considering 1 m section width, respectively. Third, to ensure the same weight per m^2 (here named as w_{slab}), an equivalent density for the slab, ρ_{eq} is used,

$$\rho_{eq} = w_{slab}/t_{eq}. \tag{4}$$

Forth, the composite section made by the steel profile and the equivalent slab should have the same composite bending stiffness as the original one. This is achieved by adding a negative offset to the equivalent slab equal to h_{eq} and computed as the weighted average of h_A and h_B (distances from the original bottom fibre to the centroid of the sections A-A' and B-B', respectively) as follows:

$$h_{eq} = (a\ h_A + b\ h_B)/(a + b). \tag{5}$$

- *Step 3: VE layer modelling.*

  The VE layer is modelled by equivalent horizontal springs. COMBIN14 ANSYS elements have been used for the model. Each horizontal spring links one node of the steel profile with one node of the equivalent slab, as depicted in Figure 5. As the VE layer is very thin, the position of both nodes could be assumed to be coincident. The stiffness of each horizontal spring, k_{eqX}, is proposed to be computed as follows:

$$k_{eqX} = \frac{G_v \; L_{el} \; b_v}{h_v}, \tag{6}$$

  where b_v and h_v are the width and the thickness of the VE layer and G_v is the assumed shear modulus for the VE material which will vary depending on the type of analysis performed with the model.

- *Step 4: Couple vertical displacement of profile and slab.*

  For the same reason above-mentioned, a constraint linear equation is also included in this model to equate the vertical displacements of both the slab and the profile.

3.1.3. Model 3: Analytical model

The analytical model used in this paper consists in a six-order PDE that describes the dynamic behaviour of a continuous sandwich beam with a VE core, as the one depicted in Figure 6. This formulation was initially proposed by DiTaranto [26] assuming the following hypothesis: (i) both of the elastic constraining layers have the same vertical displacement and curvature in bending, (ii) the VE core is modelled just considering its shear stiffness, (iii) the elastic constraining layers bend in the

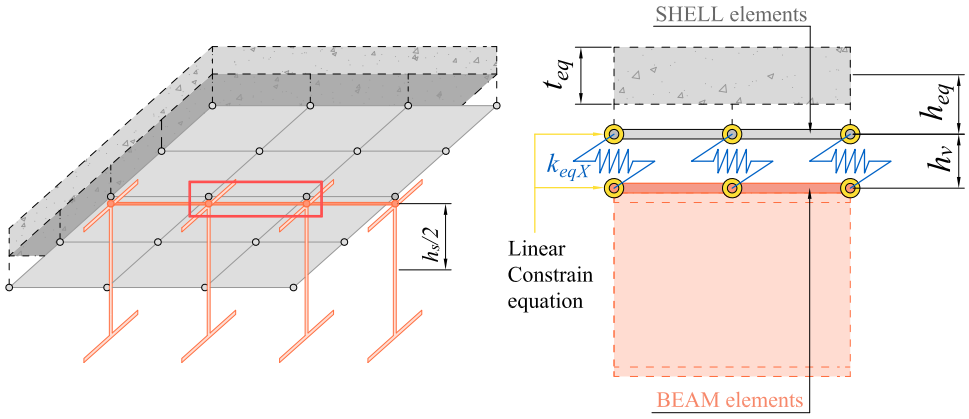

Figure 5: Model 2. Simplified Model made of BEAM, SHELL and SPRING elements.

Euler's hypothesis, (iv) the beam deflection is small and uniform across any beam section and (v) rotatory and longitudinal inertia effects are ignored.

The complex-valued free vibration problem related to this equation was solved for different boundary conditions by Rao [28]. He developed a dimensionless formulation of the sandwich beam equation based on two dimensionless parameters: the geometrical parameter Y and the complex shear parameter g^*. Parameter Y represents the percentage of additional bending stiffness achieved when both elastic layers bend as a unique monolithic section compared to when they bend as independent sections. Thus, Y may be computed as follows:

$$Y = \frac{c^2}{(E_1 I_1 + E_3 I_3)} \frac{E_1 A_1 E_3 A_3}{(E_1 A_1 + E_3 A_3)}, \tag{7}$$

where c is the distance between the centroids of both elastic constraining layers (Figure 6), E_1 and E_3 are the Young modulus of the bottom and top constraining elastic layers, respectively. I_1 and I_3 are the moments of inertia of these elastic layers, and A_1 and A_3 are their areas.

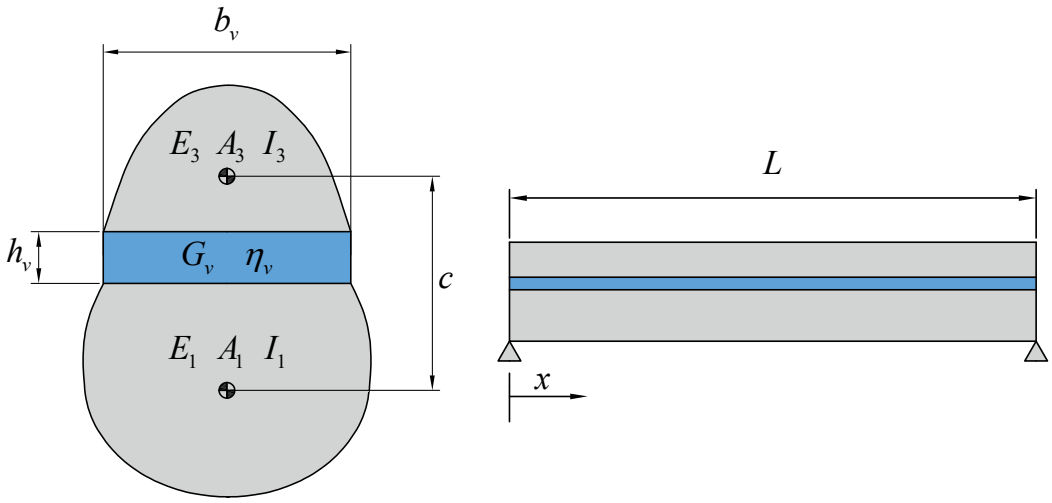

Figure 6: Model 3. *'Sandwich beam'* section studied with model 3.

Secondly, g^* is a representation of the overall shear stiffness of the VE core and is derived as shown below:

$$g^* = G'_v(1+\eta_v i)\frac{b_v}{h_v}\frac{L^2}{}\frac{(E_1A_1+E_3A_3)}{E_1A_1E_3A_3} = g(1+\eta_v i), \tag{8}$$

where L is the length of the beam considered and g is the so-called shear parameter.

When using this analytical formulation to model a secondary floor beam, the steel profile may be considered as in Step 1 of Model 2, and the rib-deck concrete slab may be modelled with the equivalent parameters previously computed in Step 2 of Model 2.

3.2. Types of modal analysis

This subsection describes three different types of modal analysis that can be applied to each type of model described in subsection 3.1.

3.2.1. Complex Modal Analysis

The CMA is considered to provide the most realistic and accurate results in terms of the beam's dynamic behaviour. In this type of analysis, the VE core material is defined with a complex-valued stiffness as the G_v^* aforementioned. The CMA provides a set of different complex circular frequencies of vibration, Ω_n^*, each one of them associated with a different complex vibration mode, $\overline{\Phi_v^*}$. When dealing with VE-damped systems, each complex frequency may be expressed in the following way [26]:

$$\Omega_n^* = \Omega_n(1 + \eta_n i)^{1/2}, \tag{9}$$

where Ω_n and η_n are the circular natural frequency and the loss factor associated with the n^{th} vibration mode, respectively. Besides, for low-damped structures, as those dealt with hereof with a damping ratio lower than 10%, η_n is accurately related to the n^{th} modal damping ratio ξ_n through:

$$\xi_n = \eta_n/2. \tag{10}$$

- *CMA for Models 1 and 2.*

  When using an FE model, the CMA consists in solving a complex generalized eigenvalue problem (as the one shown below) with a complex-valued stiffness matrix $[K^*]$ and a real-valued mass matrix $[M]$, [34].

$$([K^*] - \Omega_n^*[M])\overline{\Phi_n^*} = 0. \tag{11}$$

  Hence, when applying the CMA to the FE Models 1 and 2 the shear stiffness of the VE material has been considered to be complex and equal to G_v^*. This has

been done by first, assigning the shear storage modulus G'_v to the VE material and second, specifying the VE loss factor in the ANSYS pre-processing module. Finally, ANSYS has been commanded to perform a CMA.

- *CMA for Model 3.*

  In Model 3 the CMA has been applied through the compact formulation derived by Rao to compute the different Ω_n^* of a simply-supported sandwich beam. This formulation enables to obtain Ω_n and η_n as follows:

$$\Omega_n = \left[\frac{(n\pi)^4 + (n\pi)^2(2+Y)g + (1+\eta_v^2)(1+Y)g^2}{(n\pi)^4 + 2(n\pi)^2 g + (1+\eta_v^2)g^2}\right]^{1/2} \cdot \cdot \left[\frac{E_1 I_1 + E_3 I_3}{mL^4}\right]^{1/2} (n\pi)^2, \tag{12}$$

$$\eta_n = \frac{(n\pi)^2 g Y \eta_v}{(n\pi)^4 + (n\pi)^2(2+Y)g + (1+\eta_v^2)(1+Y)g^2}, \tag{13}$$

  where n is the index of the complex frequency to be computed and m is the mass per unit of length of the sandwich beam, and Y and g are computed using equations (7) and (8), respectively.

3.2.2. Modal Strain Energy Method

The CMA requires a complex-valued eigensolver not commonly found in every commercial structural analysis software. The MSE method enables estimating the damping ratio of a VE damped system by just using real modal analysis (always available in commercial software). This method was first applied to FE models by Johnson and Kienholz [34]. The method estimates the modal loss factor, denoted as η_{n-MSE}, of the VE damped system as a quotient of two energies: D_n the modal dissipated energy, and W_n the whole modal energy elastically stored in the system:

$$\eta_{n-MSE} = \frac{D_n}{2\pi W_n}. \tag{14}$$

The main simplification of this method lies in estimating the modal dissipated energy as follows:

$$D_n = 2\pi\eta_v W_v, \tag{15}$$

where W_v is the elastically stored energy in the VE elements of the system.

Both of these stored energies W_n and W_v are computed using the n^{th} vibration mode $\overline{\Phi_n}$ derived from a real modal analysis in which the VE material is assumed to be elastic and have an elastic shear modulus equal to the storage one G'_v. The derivation of these energies depends on whether an FE model or an analytical model is being used.

- *MSE method for Models 1 and 2.*

  In this case, $\overline{\Phi_n}$ (a column vector) is directly derived from a real modal analysis. Then, W_n and W_v are computed as follows [34]:

$$W_n = \overline{\Phi}_n^T [K] \overline{\Phi}_n, \tag{16}$$

$$W_v = \overline{\Phi}_n^T [K_v] \overline{\Phi}_n, \tag{17}$$

  where $[K]$ is the real overall stiffness matrix and $[K_v]$ is a sub-stiffness matrix that contains the contribution to the stiffness matrix of the VE elements of the structural system.

- *MSE method for Model 3.*

  Here, the Ω_n of the beam is computed with the Rao formulation assuming that η_v is equal to 0. Then, the vibration mode $\Phi_n(x)$ is derived as a mathematical function (depending on the length coordinate x) extracted from the sandwich-beam PDE (Figure 6). The involved energies to build this PDE are: (i) $(W_1 + W_3)_{bending}$ the bending strain energies of both elastic faces, (ii) $(W_1 + W_3)_{axial}$ the axial strain energy of both elastic faces, and (iii) $(W_v)_{shear}$ the shear strain energies of the VE core. These energies have been computed by corresponding integrals found in [28]. The application of the MSE method is done as follows:

$$W_n = (W_1 + W_3)_{bending} + (W_1 + W_3)_{axial} + (W_v)_{shear}, \tag{18}$$

$$W_v = (W_v)_{shear}. \tag{19}$$

From equations (14) and (15) it can be observed that the MSE method establishes a linear relation between η_v and η_{n-MSE}, however, from equation (13), it can be observed that the analytical CMA provides a non-linear relation between both magnitudes. Plotting the estimated η_n from both, CMA and MSE (Figure 7), it can be concluded that whereas for lower values of VE loss factor, η_v, the linear approximation is accurate, for higher values of η_v the MSE method considerably over predicts the beam fundamental loss factor η_1.

Current commercial VE materials used in damping applications commonly have loss factors η_v higher than 0.8 [32]. Thus, according to this, the MSE method may overestimate excessively the additional damping ratio provided by a VE treatment

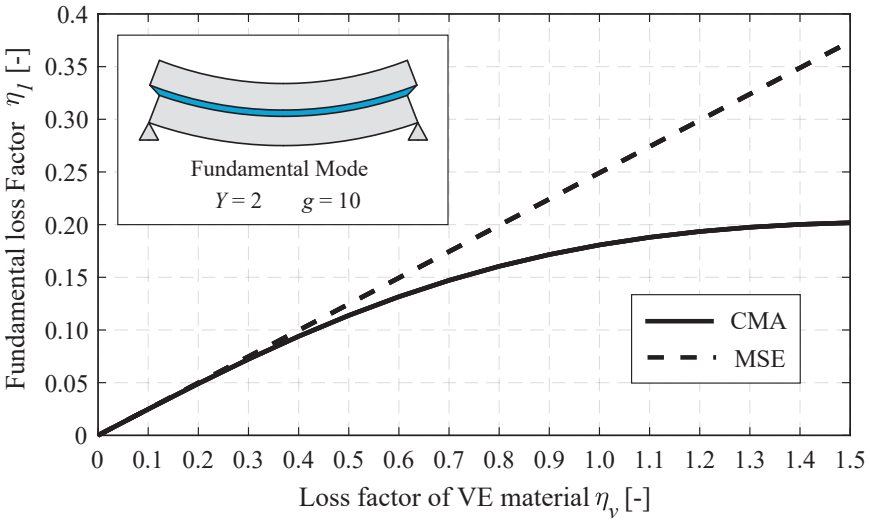

Figure 7: Loss factor of the fundamental vibration mode, η_1, of a simply-supported sandwich beam with $Y = 2$ and $g = 10$ as a function of the VE loss factor, η_v. Results computed with Model 1 using CMA and MSE.

of this nature. This fact was initially reported by Rongong [35] and further studied by Torvik and Runyon [36]. In fact, to solve this problem Rongong proposed a modification for the MSE method which will be described in the following subsection.

3.2.3. Rongong's modification to the MSE

Rongong's modification, denoted as RMSE, is based on two facts. Firstly, the proposal was based on a previous modification made by Morgenthaler [37] and named the Absolute Value MSE (AVMSE). Morgenthaler noted that the MSE always underestimated the system's natural frequency as it uses the shear storage modulus G'_v of the VE material to perform the real modal analysis. Instead of that, it was proposed to perform the MSE with the modulus of the complex shear modulus $|G^*_v|$ which represents more realistically the actual stiffness of the VE material. Secondly, Rongong

realized that a correction had to be made in the modal energies derived from using $|G_v^*|$ to provide a better approximation to the actual strain energies involved in the MSE.

When simply applying the AVMSE method, a modal loss factor, here named as $\eta_{n-AVMSE}$, is obtained. The modal loss factor given by the RMSE, η_{n-RMSE}, can be related to this latter as follows:

$$\eta_{n-RMSE} = \frac{1}{\left(\frac{1}{\eta_v} + \sqrt{1+\eta_v^2}\left(\frac{1}{\eta_{n-AVMSE}} - \frac{1}{\eta_v}\right)\right)}. \tag{20}$$

Moreover, Torvik and Runyon proved that the RMSE method always slightly underestimates the system loss factor, which results to be really convenient when predicting the additional dissipative capacity provided by a damping treatment at the design stage.

3.3. Comparison between the different modelling approaches

As a result of combining the 3 types of models with the 3 types of analysis above described, 9 modelling approaches may be defined. These are listed in Table 1.

Table 1: The 9 different modelling approaches compared.

Modelling Approaches	Model 1: Detailed FE	Model 2: simplified FE	Model 3: Analytical
CMA	M1-CMA	M2-CMA	M3-CMA
MSE	M1-MSE	M2-MSE	M3-MSE
RMSE	M1-RMSE	M2-RMSE	M3-RMSE

Within them, the approach M2-RMSE (which employs the simplified FE Model 2, analysed with the RMSE method) is the one proposed in this paper as a simple

but accurate enough modelling approach for practitioners to model the damping behaviour of the studied CLD-treated floor beams. M1-CMA has been considered to be the approach providing the most accurate and realistic results.

The benchmark beam defined in Section 2 has been used to compare the 9 modelling approaches. For that, the fundamental modal parameters of this beam (its fundamental natural frequency $f_1 = \Omega_1/(2\pi)$ and its fundamental loss factor η_1) have been obtained within each approach for different shear stiffness of the VE core,i.e. varying the shear parameter g of the beam through varying the G_v' of the VE material . This is a common practice in the field of CLD treatments as it is well known that there is an optimum shear stiffness which provides the maximum dissipation capacity to the sandwich beam [17]. It is a common practice to modify g by varying h_v or b_v and keeping G_v' constant. However, in this paper, the authors preferred to vary G_v' to maintain constant the geometry of the CLD treatment along each studied beam. Throughout the whole study, g has been computed using equation 8 no matter which model M1, M2 or M3 has been used.

The research performed in this paper is limited to the fundamental modal parameters of floor beams, as the fundamental mode is the main contributor to the final dynamic response of the floor under human-induced excitation. Despite this fact, the methodology developed in this paper is also applicable for estimating higher-order modal parameters which could be relevant in other structural types or under different dynamic excitation sources, such as machine-induced vibrations.

This comparison is depicted in Figures 8a and 8b in which the results of each modelling approach are represented with a line characterized by a colour (defining the type of model) and a type of line (defining the type of analysis). In both figures, the optimal region around the maximum loss factor has been zoomed in. Additionally, Figures 9a and 9b depict, for each type of model, the relative errors when predicting

f_1 and η_1 with the MSE and RMSE compared to the values provided by the CMA.

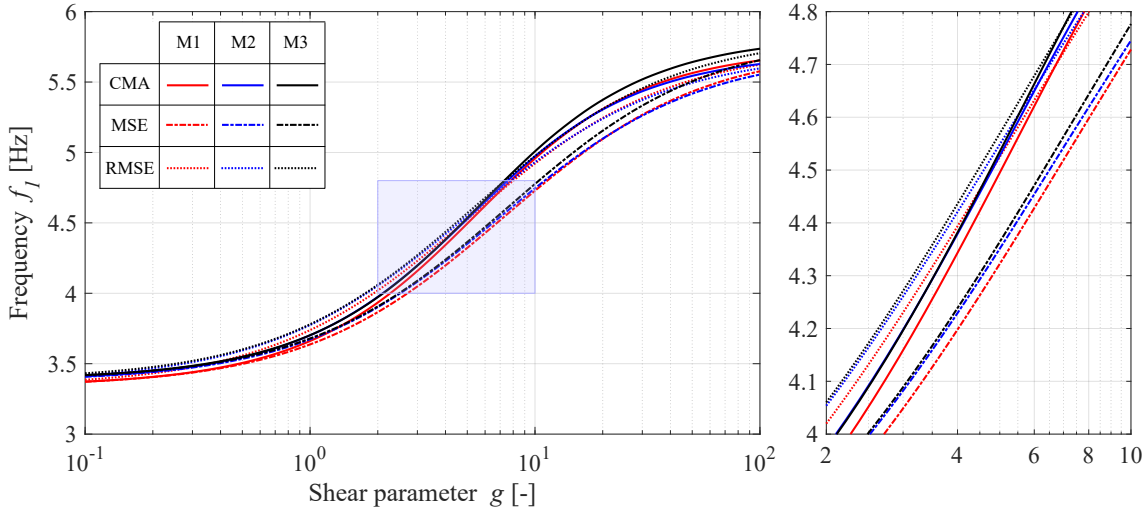

(a) Fundamental natural frequency of the beam f_1

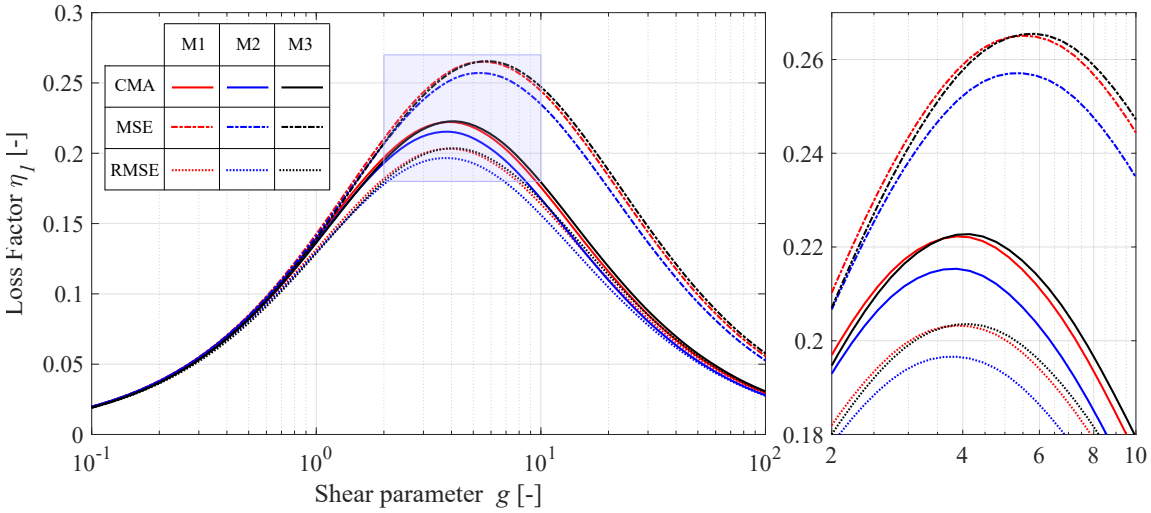

(b) Fundamental loss factor of the beam η_1

Figure 8: Comparison of the dynamic parameters of the beam predicted with the 9 different modelling approaches as a function of the shear stiffness of the VE core.

From Figures 8 and 9, the following conclusions may be extracted. First, models

M1, M2 and M3 provide similar results when using the same type of analysis. It is important to highlight that the equivalent constant-height slab used in models M2 and M3 provides similar results to the rib-deck slab modelled in detail in M1. M2 provides lower values of η_1 (with deviations smaller than 5% when compared to model M1) while the fundamental natural frequency is almost identical for both modelling approaches.

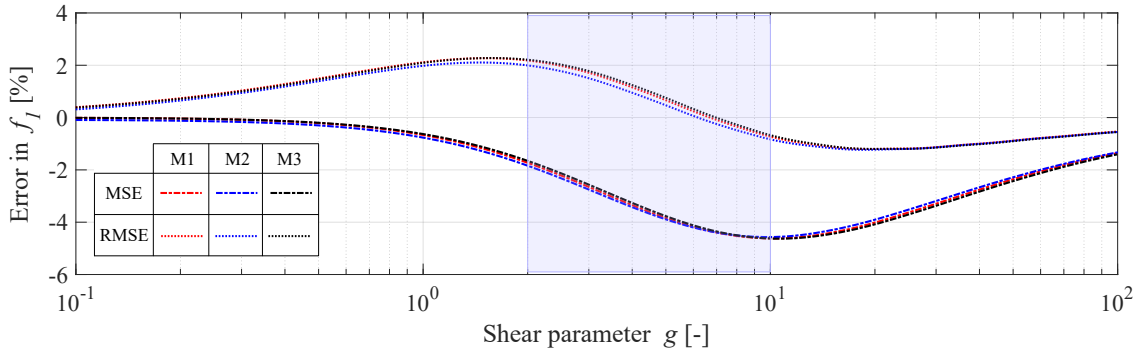

(a) Error in the fundamental natural frequency of the beam f_1

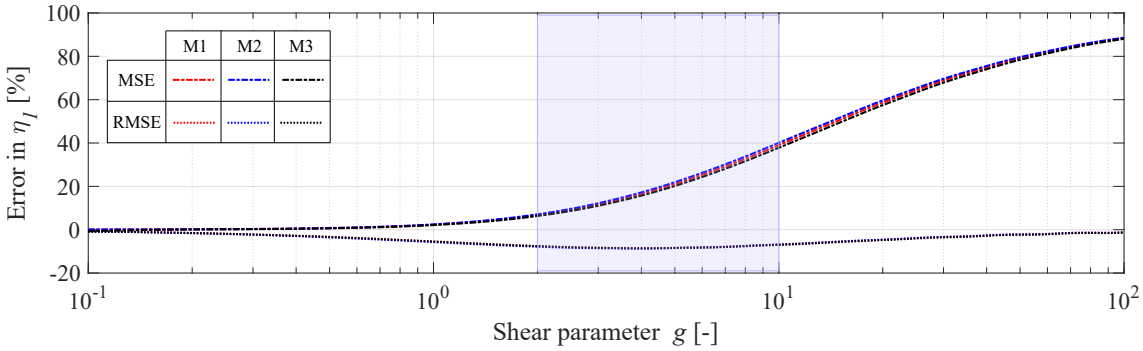

(b) Error in the fundamental loss factor of the beam η_1

Figure 9: Error given by the MSE and RMSE compared to CMA.

Regarding the type of analysis, on the one hand, when compared to the CMA, the MSE always underestimates f_1 (with a limited error of -5%, Figure 9a), over

predicts η_1 (providing errors of up to +40% in the zoomed-in region, Figure 9b) and overestimates the optimal value of g reaching an error for this case of +50% (see zoom in Figure 9b). On the other hand, the RMSE method provides limited errors of f_1 (smaller than +2%, Figure 9a), always underpredicts the value of η_1 (reaching errors of around -10% in the range of maximum damping, Figure 9b) and computes the optimal value of g accurately (see zoom in Figure 8b). Thus, the RMSE is accurate enough to estimate at the design stage the additional damping ratio provided by the CLD treatment while remaining on the safe side. Finally, when comparing the proposed modelling approach, M2-RMSE, with the most accurate one, M1-CMA, the maximum error achieved in η_1 is -12%, which is small enough for engineering design purposes. Furthermore, the approach M2-RMSE offers a methodology that considerably reduces the number of nodes and elements in the FE model. In this study, this has meant decreasing by a factor of 10 the time needed to generate and mesh the geometry of the model, and by a factor of 4 the time needed to perform the modal analysis and expand the beam's vibration modes. This fact can be useful when using large structural FE models or when developing parametric or sensitivity analysis to accurately design the applied CLD treatment, as in these cases, a model of the floor needs to be run many times.

To sum up, a flowchart for the development of the modelling approach M2-RMSE has been included in Figure 10 and can be summarized in the following steps:

1. Model the steel profile with an offset.
2. Compute an equivalent constant-height slab for the rib-deck slab.
3. Model the slab with an offset.
4. Compute the equivalent stiffness of the spring elements used for the VE layer. An elastic stiffness for this layer considering the absolute value of the complex

shear modulus is assumed.

5. Model the VE layer with spring elements.
6. Couple the vertical displacement of the steel profile and the concrete slab.
7. Perform a real modal analysis.
8. Compute the η_{AVMSE}.
9. Compute the η_{RMSE}.

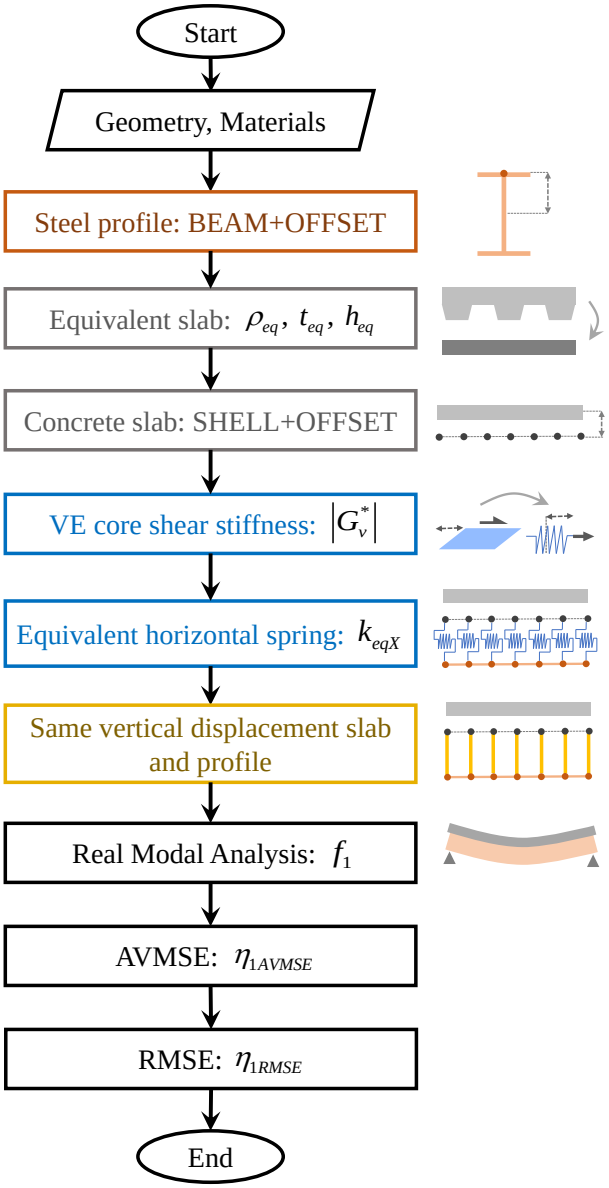

Figure 10: Flowchart for M2-RMSE approach.

4. Parametric study

A parametric study is conducted for studying the dynamic behaviour of partially treated composite beams, that is, the CLD treatment is only applied for a percentage of its length. Both approaches, M1-CMA and M2-RMSE, have been used to further check the accuracy of the second one. In this section model M3 has been excluded from the study, as it has already been proven its correlation with the FE models used in the previous section. Additionally, the inclusion of M3 would imply complex challenges related to the solution process of the equation of DiTaranto for partially treated beams, which are not within the scope of the paper.

4.1. Studied cases

The set of composite beams partially treated is depicted in Figure 11 in which the variation range of the studied parameters is shown. Regarding material properties, a lightweight concrete LWC25 with a characteristic compressive strength $f_{ck} = 25$ MPa was chosen. A steel S275 with a yielding stress f_y =275 MPa was used for profiles. Finally, the VE layer was defined with a constant loss factor $\eta_v = 1$ and its complex shear modulus G_v^* is varied for each case.

In terms of geometry, two parameters have been varied: first, the beam length L which adopted values of 6, 9, 12 and 15 m; and second, the percentage of beam length (L_v in Figure 11) treated with CLD which has been varied from 0% to 100%, each 10%. The concrete slab geometry has remained constant and has been defined with a steel rib-deck Cofraplus 60 with 1.2 mm gauge, a width $b_c = 3.00$ m and a full height $h_c = 0.12$ m. For the CLD, two 1mm steel sheets and a 1mm VE layer between them have been considered. The width of the CLD treatment has been considered equal to the width of the steel profile.

For each beam resulting from combining a given L, and a given $\%CLD$, the lightest steel profile from the Universal Beams (UB) series that fulfils the static design criteria of the partially treated beam is chosen. For that, a simply-supported beam scheme together with a Dead Load (DL) of 1 kN/m^2 and a Live Load (LL) of 4 kN/m^2 are used. This design complies with Ultimate Limit State (ULS) and Deflection Serviceability Limit State (DSLS) according to Eurocode 4 [38]. When $\%CLD = 0$, the resisting section is the composite one, while when $\%CLD = 100$, this section is composed only of the steel one. However, when $\%CLD$ is in between, a beam with a partially connected length arises, so special attention must be paid to these limit states. Some important aspects in this respect are covered in the following subsections.

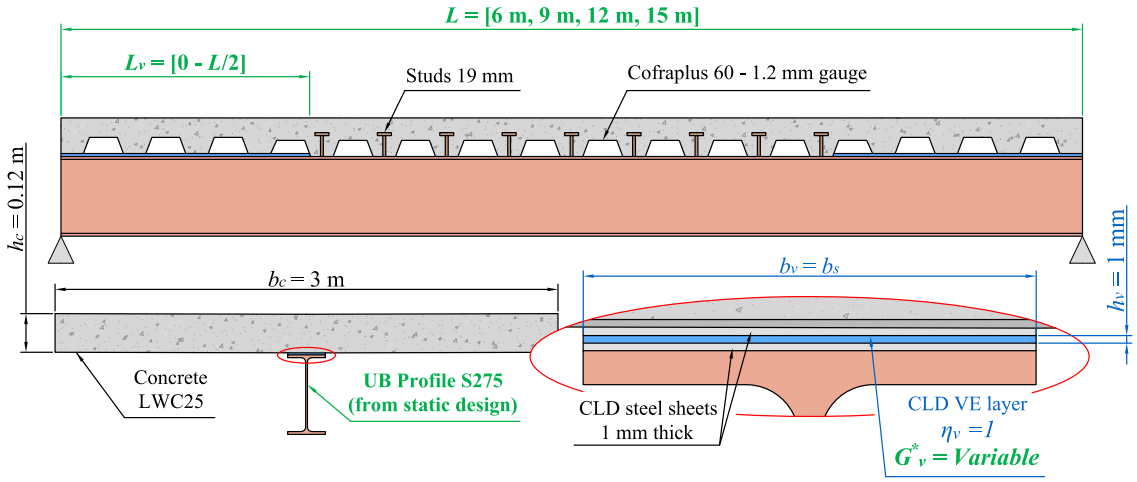

Figure 11: Parameters that define each partially treated composite beam for the parametric study (green parameters are those varied along the set of cases).

The parametric study performed is composed of 4 x 11 = 44 beams, each one of them resulting from combining a length L, a $\%CLD$ and an appropriate UB profile.

Finally, the dynamic characteristics of each beam have been extracted with M1-CMA and M2-RMSE for different shear stiffnesses of the VE core, G_v^* and $|G_v^*|$, respectively.

4.1.1. Bending ULS of beams with partial connected length

For this limit state, the following hypothesis are assumed: i) for sections of the beam without shear connection to the slab, the resisting bending moment is the plastic bending moment of the steel profile, and ii) for the mid-span section, the composite action with the concrete slab is considered as follows:

- The effective breath of the composite slab has been computed as follows:

$$b_{effc} = \min \left\{ \begin{matrix} (L - 2L_v)/4 \\ b_c/2 \end{matrix} \right\}. \tag{21}$$

  The effective breath typically used for simply-supported beams [38], but replacing the beam length, L, by the connected length $L_c = (L - 2L_v)$ (this assumption is on the safe side).

- The use of ductile shear connectors of diameter 19 mm with rigid-plastic behaviour has been assumed.

- Partial shear connection theory has been used [38]. Thus, the compressive plastic stress block with a resultant axial force N_c in the concrete slab is reduced (with respect to the case with full shear connection) by a factor called 'degree of shear connection' denoted here as α (although in EC4 is named η) and computed as follows:

$$\alpha = \frac{P_{rd}(n/2)}{N_{cf}}, \tag{22}$$

$$N_c = \alpha N_{cf}, \tag{23}$$

where P_{rd} is the design value of the shear resistance of a single shear connector, N_{cf} is the resulting axial load in the concrete slab for the full shear connection case, and n is the total number of shear connectors used within the connected length of the beam.

4.1.2. DSLS of the beam with partial connected length

For the DSLS, two different bending stiffnesses along the beam are used: i) the one from the steel profile for the disconnected region, and ii) the one from the full composite cracked section for the central region assuming the same effective breadth described before.

4.2. Results

4.2.1. Modal parameters depending on g

Firstly, the modal parameters of each beam, namely, f_1 and η_1 have been obtained as a function of g (computed in the same way as before). Figure 12 shows an example for beams with 9 m of span and different $\%CLD$.

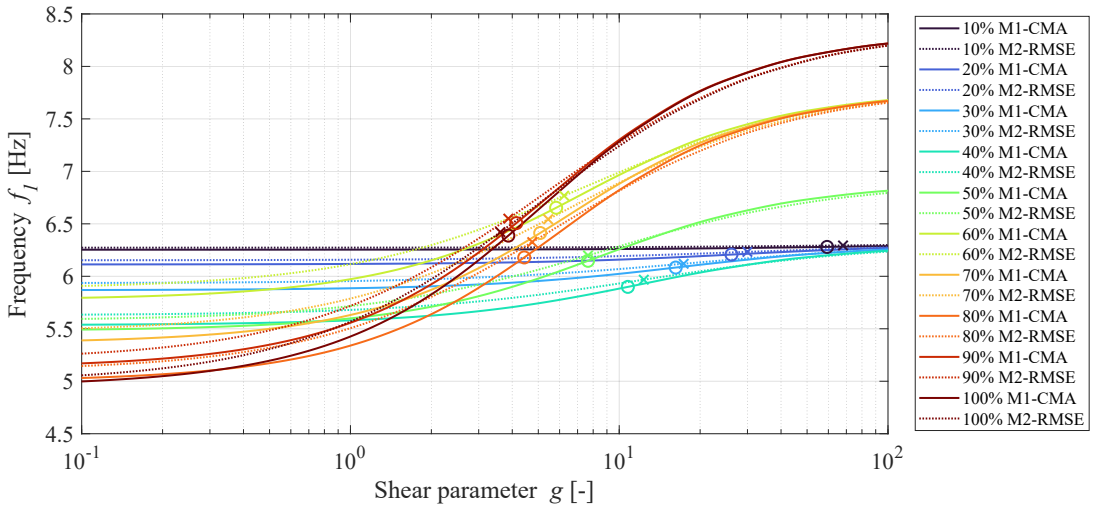

(a) Fundamental natural frequency of the beams f_1

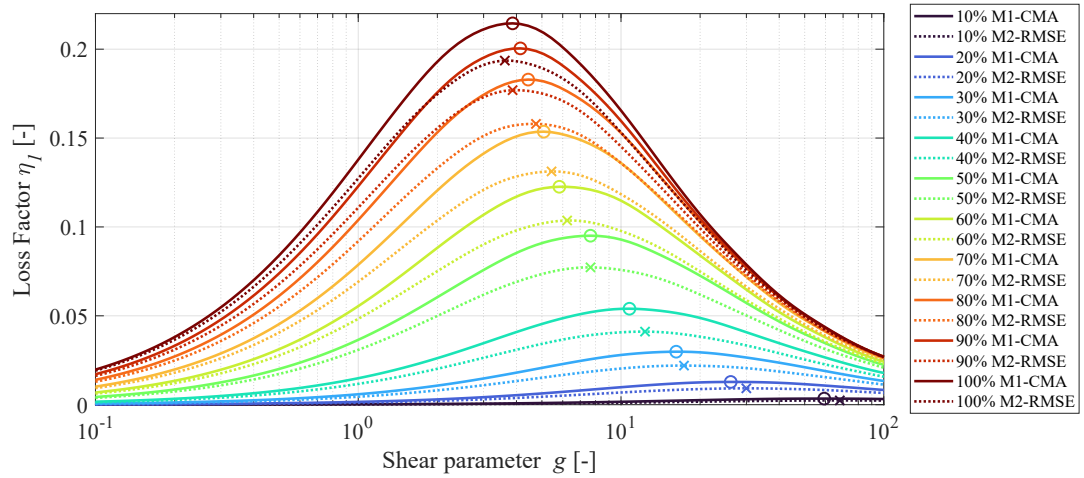

(b) Fundamental loss factor of the beams η_1

Figure 12: Parametric study of fundamental modal parameters varying g for 9 m span beams with different $\%CLD$ and computed with M1-CMA and M2-RMSE approaches.

Charts with similar behaviour have been obtained for beams of 6, 12 and 15 m

span. Some conclusions may be extracted from Figure 12a. First, the higher the $\%CLD$, the wider the frequency range along which the beam varies (Figure 12a). Second, M2-RMSE predicts accurately the beam frequency. Third, from the optimal points it can be seen that the optimal frequency does not change significantly when increasing the $\%CLD$. This occurs because the loss of stiffness caused by the CLD treatment is compensated with the use of a stiffer UB profile.

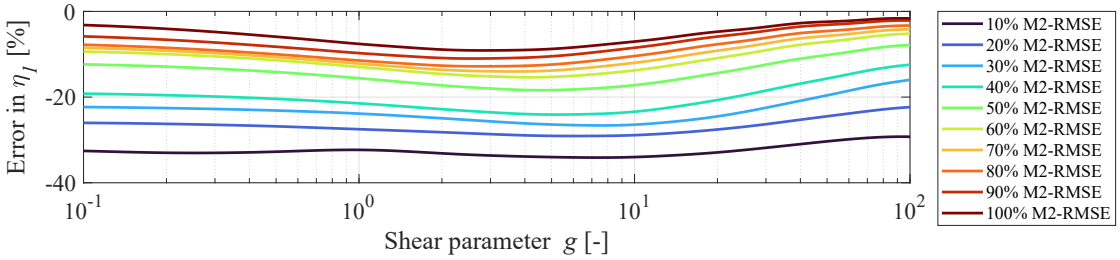

Figure 13: Error in the fundamental loss factor as a function of g for 9 m span beams for different $\%$ CLD when using M2-RMSE compared to M1-CMA.

Concerning Figure 12b and Figure 13 the following aspects can be remarked. First, the loss factor of the beam increases as the $\%CLD$ increases, and furthermore, the η_1 - g curve for a given $\%CLD$ is an envelope for those of lower $\%CLD$. Second, it can be seen that when the $\%CLD$ is lower than 30%, the increase in damping is marginal. Third, the values of η_1 predicted by the M2-RMSE are slightly lower than those predicted by M1-CMA (Figure 13) which is on the safe side. This difference becomes higher for lower $\%CLD$ reaching a maximum error of -35%. Nevertheless, this value corresponds to a relative error and occurs for lower values of $\%CLD$ and thus, it is associated with a small absolute error. This implies that to the authors' experience, the proposed methodology is applicable for all ranges of $\%CLD$, as it provides reasonable estimations of the beams' damping ratios in absolute terms.

4.2.2. Optimal modal parameters

The optimal values achieved in Figure 12 are now analyzed. Three parameters have been studied: the optimal frequency f_{opt}, the optimal loss factor η_{opt} and the optimal shear parameter g_{opt}. Figure 14 shows these parameters for the 4 considered spans with different $\%CLD$.

The following conclusions can be derived. First, Figure 14a shows that the f_{opt} is approximately constant with $\%CLD$ and the error of M2-RMSE is very low and decreases with the span (Figure 14b). Second, Figure 14c shows that the value of η_{opt} with $\%CLD$ for different beam spans is similar. Despite this fact, the shorter the span, the slightly higher the value of η_{opt}. That is, shorter-span beams have smaller UB profiles, and thus, the resulting *'sandwich beam'* section has slightly higher values of Y. This means that the increase of bending stiffness achieved when connecting to shear short-span beams is higher than for long-span beams (where most of the stiffness of the composite section comes from the steel profile). According to Equation (13) the higher the value of Y, the higher η_{opt} is, which explains the slight increase of η_{opt} for short-span beams. In addition, in Figure 14d, it can be seen that the absolute value of the error of η_{opt} is higher for short-span beams.

Third, from Figure 14e, it is also relevant to remark that the variation of g_{opt} with $\%CLD$ is similar for the different spans, being slightly higher for short-span beams. This can be explained again in terms of dimensionless parameters, since g_{opt} depends directly on Y. The M2-RMSE always overpredicts slightly the value of g_{opt} and this error reduces when $\%CLD$ increases.

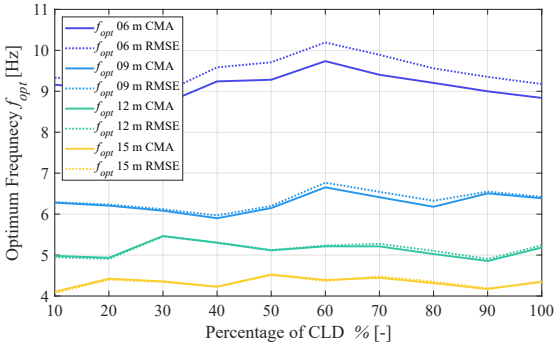

(a) Optimal natural frequencies, f_{opt}

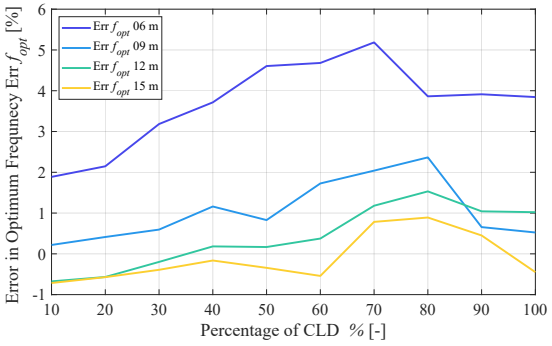

(b) Error of M2-RMSE in f_{opt}

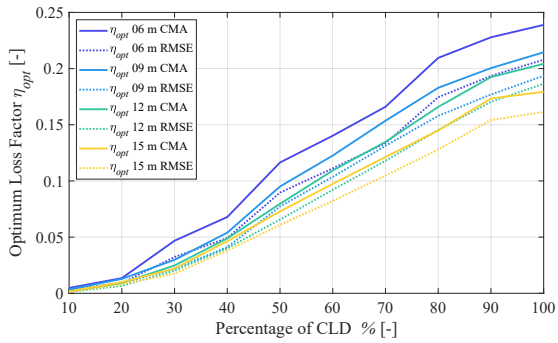

(c) Optimal loss factor, η_{opt}

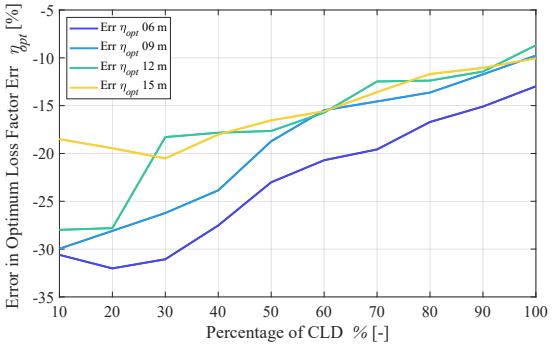

(d) Error of M2-RMSE in η_{opt}

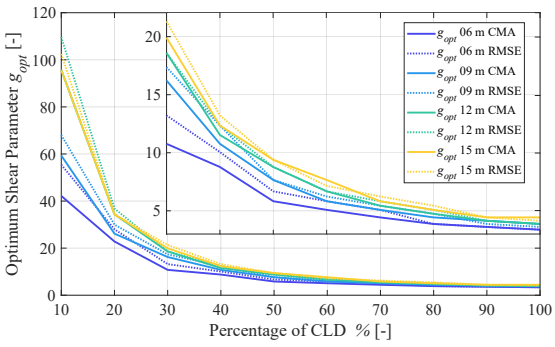

(e) Optimal shear parameter, g_{opt}

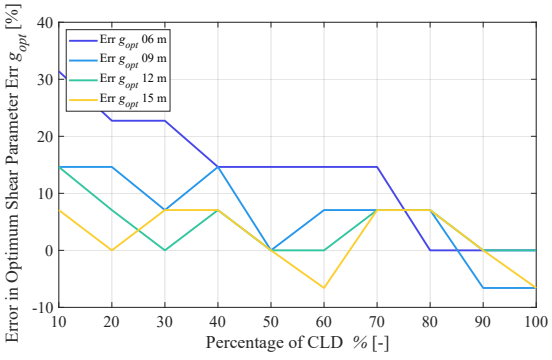

(f) Error of M2-RMSE in g_{opt}

Figure 14: Optimal modal parameters for different beam spans and $\%CLD$. Comparison of predictions made with M1-CMA and M2-RMSE.

5. Application example: dynamic response of single-spanning composite floors with and without CLD

The results obtained in Section 4.2.2 have been used to predict the dynamic response of single-spanning floors subjected to human walking. Each floor is composed of one bay of secondary beams, all of them simply-supported in columns disposed each 3m (a distance equal to the slab width used for the parametric study). Thus, the modal parameters of the beams previously studied can be used to predict the dynamic response of these floors. A scheme of the floor structural layout is included in Figure 15a.

The floors' dynamic response has been assessed in terms of i) the response developed by a low-frequency floor when resonates with a given harmonic of the human dynamic load, and ii) the impulsive response after a human footfall (usually used to assess the VSLS of high-frequency floors). For that, the recommendations given in [39] have been followed, as this guideline has proven to provide a well-calibrated methodology to assess the VSLS in composite floors according to the research done by [40] and [4]. Additionally, to demonstrate the effectiveness of CLD treatments at the design stage of lightweight floors, a second set of floors without CLD has been assessed for comparison. For these, a stiffening strategy based on increasing the steel profile of the floor is used to reduce their dynamic response.

5.1. Resonant response of low-frequency floors

The fundamental vibration mode of the floor is considered for the resonant response. Therefore, these floor parameters are needed: i) the fundamental natural frequency, in each case assumed to be equal to f_{opt} computed with M1-CMA, ii) the damping ratio of the floor assumed to be $\xi_{opt} = \eta_{opt}/2$ (computed with M1-CMA),

and, iii) the effective weight associated to the fundamental vibration mode at its anti-node, W_{eff}. The latter has been computed assuming an effective floor area which is involved in the dynamic response (as depicted in Figure 15b) [39]. Its effective length has been considered equal to the beam length, L, and its width B_{eff} is computed as follows:

$$B_{eff} = 2\left[\frac{EI_{slab}}{EI_{beam}}\right]^{\frac{1}{4}} L, \tag{24}$$

where EI_{slab} is the flexural stiffness of the slab and EI_{beam} is of the secondary beam. The latter one is derived from the formula for the fundamental frequency of a simply-supported beam as follows:

$$EI_{beam} = \frac{4 f_{opt}^2 L^4 m}{\pi^2}, \tag{25}$$

where m is the mass per unit of length of the beam.

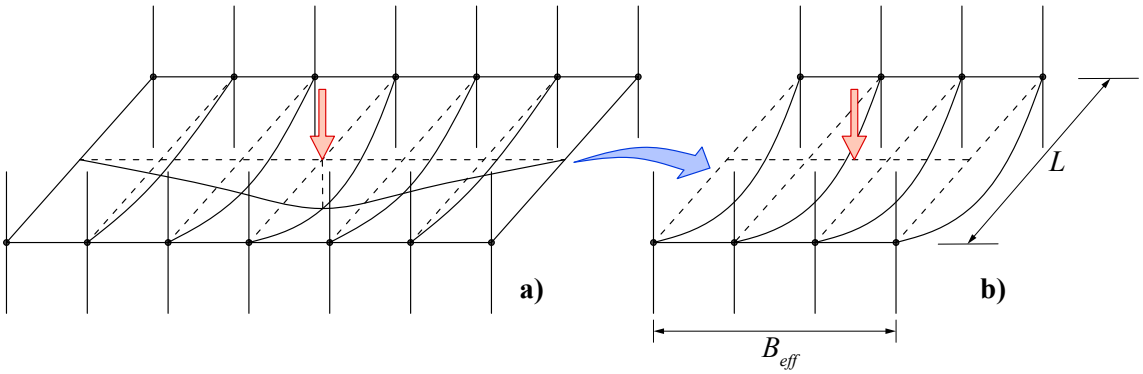

Figure 15: Layout of the single-spanning floors assessed. Conceptual representation of the effective floor area involved in the floor response.

Then, the effective weight of the floor is obtained as follows:

$$W_{eff} = 0.5\ w\ B_{eff} L, \tag{26}$$

where the 0.5 factor is used to consider the vibration mode of a single-spanning simply-supported floor and w is the weight per unit of area of the studied floor derived from the following equation:

$$w = w_{slab} + \frac{w_{prof}}{b_c}, \tag{27}$$

where w_{prof} is the weight per unit of length of the steel profile used in the floor.

A harmonic load is applied at the anti-node of the fundamental mode of vibration with a frequency equal to the fundamental natural frequency of the floor:

$$F_h(t) = Q\ \alpha_h \sin(2\pi f_{opt} t), \tag{28}$$

where Q is the weight of a human assumed to be 700 N and α_h is the dynamic loading factor depending on the loading frequency as follows:

$$\alpha_h = 0.83\ e^{-0.35 f_{opt}}. \tag{29}$$

The response has been computed in terms of peak acceleration according to the expression proposed by the Guideline [39] as follows:

$$a_{p-res} = \frac{R_{cres}\ Q\ 0.83\ e^{-0.35 f_{opt}}}{2\xi_{opt}\,(W_{eff}/a_g)}, \tag{30}$$

where R_{cres} is a calibration reduction factor with a value of 0.7 and a_g is the acceleration of gravity.

The peak acceleration can be transformed into a root-mean-square (rms) value, $a_{rms-res}$, by dividing it by a crest factor equal to $\sqrt{2}$. Finally, the response factor

R_{res} can be computed by dividing the $a_{rms-res}$ by a base rms acceleration value equal to 0.005 m/s^2 according to [41].

$$R_{res} = \frac{a_{rms-res}}{0.005}. \tag{31}$$

5.2. Impulsive response after a human footfall

The impulsive response is also computed according to the formulation proposed in [39]. The same floor parameters previously computed are used for that. Hence, the effective impulse, I_{eff} (with units of [Ns]) is applied at the anti-node of the fundamental vibration mode as a load model:

$$I_{eff} = 42 \left(\frac{f_{step}^{1.43}}{f_{opt}^{1.30}} \right), \tag{32}$$

where f_{step} is the human pacing frequency here assumed to be 2.6 Hz (as higher pacing frequencies provide higher impulsive responses [41]). Thus, the impulsive response is composed of a peak acceleration a_{p-imp} followed by a decaying response that lasts till the next footfall occurs, during a time equivalent to the pacing period. The rms acceleration of this response $a_{rms-imp}$ can be computed as follows:

$$a_{p-imp} = \frac{2\pi f_{opt} R_M I_{eff}}{(W_{eff}/a_g)}, \tag{33}$$

$$a_{rms-imp} = \frac{a_{p-imp} R_{cimp}}{\sqrt{2}} \sqrt{\frac{1 - e^{-4\pi (f_{opt}/f_{step}) \xi_{opt}}}{\pi (f_{opt}/f_{step}) \xi_{opt}}}, \tag{34}$$

t where R_M is a higher mode factor equal to 2, and R_{cimp} is a calibration factor equal to 1.3.

The response factor R_{imp} is again derived according to [41] as follows:

$$R_{imp} = \frac{a_{rms-imp}}{0.005} \ (f_{opt} < 8 \text{ Hz}) \,,$$
$$R_{imp} = \frac{a_{rms-imp}}{2\pi f_{opt}\, 0.0001} \ (f_{opt} > 8 \text{ Hz}) \,. \tag{35}$$

5.3. Results of the dynamic behaviour of floors with and without CLD

The results obtained by following the procedure explained in subsections 5.1 and 5.2 are depicted in Figure 16 where the response factor of each floor assessed has been plotted against the mass of the steel profile per meter, m_{prof} used in the floor. Blue curves correspond to floors treated with CLD while black ones are stiffened floors without CLD treatment. Continuous lines represent the resonant floor response while the dotted ones represent the impulsive response. Furthermore, the identification of the UB profile used in each case is included next to their impulsive response, and, in the case of CLD-treated floors, the $\%CLD$ is also included next to the dot. For clarification, the same data plotted in blue lines can be found in a numeric format in Appendix A. Moreover, some graphs have red sections indicating that the methodology used to compute the response on that specific floor was not calibrated for its natural frequency (which has also been included). In the case of the 6m span floors, only the impulsive response has been computed as their natural frequencies were always over 10 Hz.

From Figure 16 it can be seen that the amount of steel needed to obtain the same level of dynamic response is much lower when including CLD treatments than when stiffening the floor. On the one hand, in CLD treated floors, m_{prof} increases a 50% when $\%CLD$ increases from 0% to 100% (e.g. from 82 kg to 125 kg in 15 m beams in Figure 16d, or from 60 kg to 82 kg in 12 m beams in Figure 16c), however, R_{res}

drastically decreases from 8 to 1 for 12 m and 15 m beams (Figures 16c and 16d) and R_{imp} decreases from 8.5 to 5.5 in 15 m beams (Figure 16d), or from 16 to 7 in 9 m beams (Figure 16b). On the other hand, the stiffening strategy is competitive for 6 m beams (Figure 16a) where the frequency of the floor increases fast as the floor is stiffened (despite CLD treatments still providing better designs in this case). Although, for 12 m and 15 m floors, the amount of additional steel mass needed to reach the same vibration reduction as the one obtained with CLD is around 120% to 140% (e.g. from 60 kg to 134 kg in 12 m floors, Figure 16c, or from 82 kg to 201 kg in 15 m floors, Figure 16d).

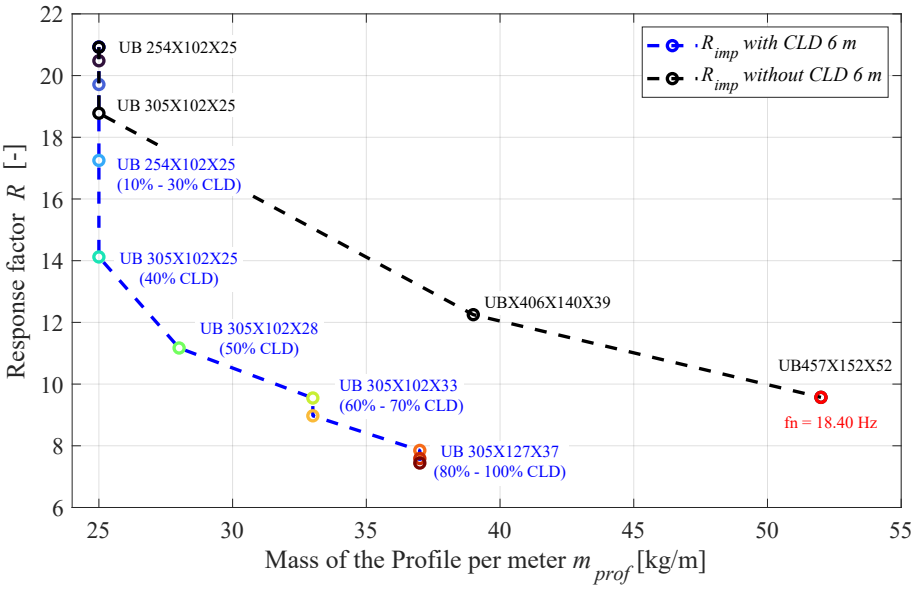

(a) Response of floor with 6 m span.

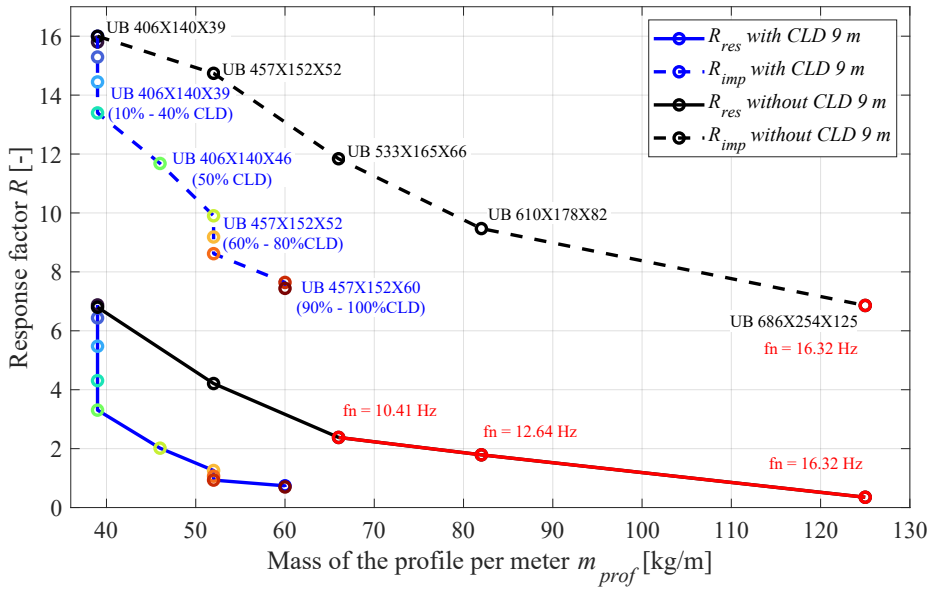

(b) Response of floor with 9 m span.

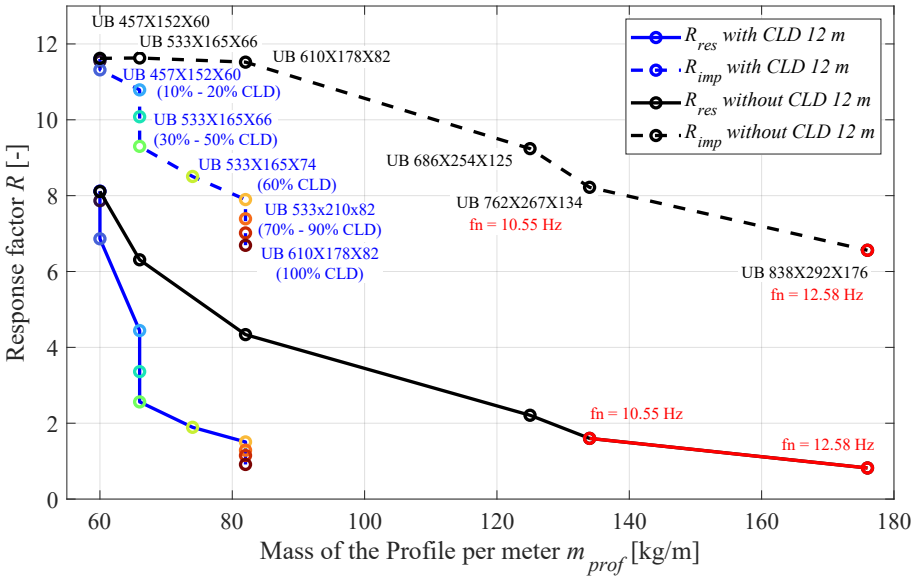

(c) Response of floor with 12 m span.

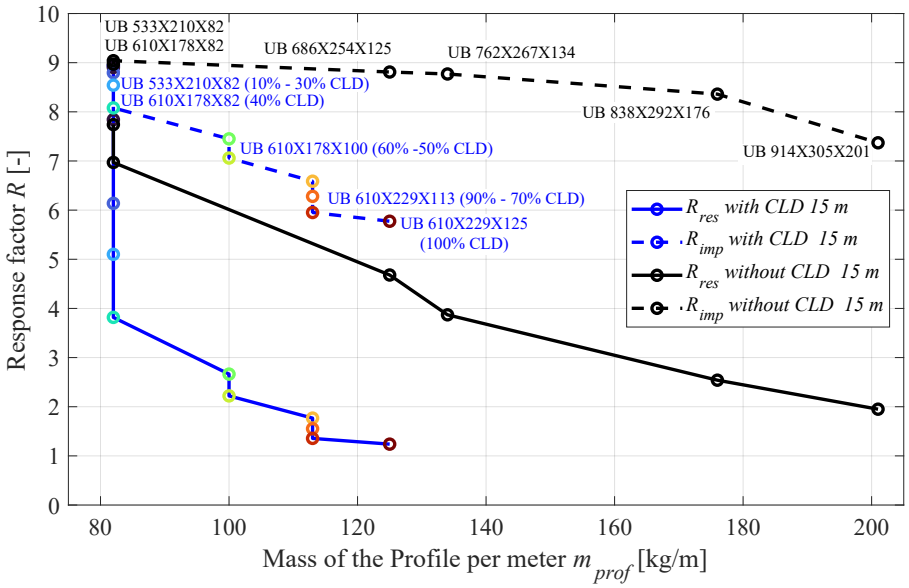

(d) Response of floor with 15 m span.

Figure 16: Response factors R_{res} and R_{imp} of assessed beams with and without CLD treatment as a function of the mass of the steel profile used in the floor m_{prof}.

6. Conclusions

This paper provides a detailed analysis of the additional damping ratio provided by VE CLD treatments applied to composite floor beams. The studied CLD treatment consists of a thin VE layer (1mm thick) included between the steel beam and the concrete slab of a composite beam and applied for a proportion of its length near the supports, leaving its central region connected to shear.

First of all, 3 types of models combined with 3 types of analysis have been used to predict the dynamic characteristics of a case-study beam fully treated with CLD along its overall length. All of them provided similar results. From here, two modelling approaches, i) the most complex one, named M1-CMA (with detailed geometry, SOLID elements and using Complex Modal Analysis (CMA)) and the proposed modelling approach named M2-RMSE (with spring elements to model the VE layer and using a modified MSE method) were chosen to develop a parametric analysis. This was developed by combining different beam lengths (6m, 9m, 12m and 15 m) with different percentages of CLD treatment (from 0% to 100% each 10%). First, It was observed that treatments with $\%CLD$ lower than 30% may not be useful due to the reduced additional damping provided. Second, the M2-RMSE always underpredicted the loss factor of the beams, with maximum mismatches with respect to M1-CMA of around -35%. Additionally, the higher the $\%CLD$ and the higher the beam length, the lower this mismatch. Thus, it has been concluded that the approach M2-RMSE is simple and accurate enough for engineering purposes, especially for optimization processes in which many models need to be run to reach a satisfactory solution. This paper also provides a detailed step-by-step procedure to accurately develop this modelling approach for practitioners to easily integrate this damping technology in future designs of lightweight floors.

Finally, a dynamic response analysis of single-spanning floors composed of the analysed beams was developed as an application example. The set of CLD-treated floors was compared to a second set of floors in which the vibration level was reduced by stiffening the steel profile of the floor. It was concluded that the CLD treatments enable the development of lighter and more slender floors with less use of steel for the same level of vibration. Hence, the CLD treatment when properly designed is an efficient tool to reduce the embodied carbon of long-span composite floors sized by the VSLS.

The results shown here shed light on the practical ways of modelling CLD treatments applied to civil engineering purposes and on their effectiveness when designing vibration-sensitive floors. Future works will be focused on applying this knowledge to integrate the CLD technology into long-span timber floors especially sensitive to vibration. Additionally, further optimization of two-spanning composite floors with integrated CLD treatments will be researched in order to reduce the carbon footprint of these structural systems.

7. Acknowledgements

The authors acknowledge Grant PID2021-127627OB-I00 (Transport Infrastructures subjected to dynamic loading: assessment techniques for the sustainability, intelligent maintenance and comfort) funded by Ministerio de Ciencia e Innovación, Agencia Estatal de Investigación and 10.13039/501100011033 FEDER, European Union.

Appendix A. Tables with Results of CLD-treated beams

These tables present the numeric results depicted in Figures 14 and 16. Each table corresponds to a beam length analyzed, L. Each row provides the information for each studied case resulting from combining a beam length L with a given $\%CLD$. The lightest UB profile that satisfies the static design of the beam analyzed is included for each case. The geometry parameter Y of each beam section is also presented. The next columns correspond to the dynamic parameters of the beam optimally treated, f_{opt}, η_{opt} and to the optimal shear parameter of each CLD treatment g_{opt}, all of them presented in Figure 14. To conclude the Table presents the results depicted in Figure 16: the resonant response of CLD-treated floors, R_{res}, and their impulsive response R_{imp}. Every parameter presented has been computed using both approaches, M1-CMA (values at the left side of each cell) and M2-RMSE (values on the right side).

The parameter $\%CLD_{est}$ corresponds to the percentage of CLD that it is aimed to be analyzed in each case. However, as the concrete slab is defined with a rib-deck with ribs of a given length in M1-CMA, only certain discrete percentages of CLD may be studied. Thus $\%CLD_{real}$ corresponds to the closest higher real $\%CLD$ that can be assessed.

Table A.2: 9 Numeric results of parametric study.

GEOMETRY		L [m]	% CLD_{ext} | % CLD_{real}	UB PROFILE	Y [-]	f_{mopt} M1-CM4 | M2-RMSE	η_{opt} M1-CM4 | M2-RMSE	g_{opt} M1-CM4 | M2-RMSE	R_{imp} M1-CM4 | M2-RMSE	R_{res} M1-CM4 | M2-RMSE
Length [m]	6	6	0 | 0	UB 254X102X25	2.35	9.30 | 9.30	0.0000 | 0.0000	-	20.93 | 20.93	5.26 | 5.26
Ribdeck Slab Type	Cofraplus 60		10.00 | 14.57	UB 254X102X25	2.35	9.15 | 9.33	0.0048 | 0.0033	42.18 | 55.43	20.48 | 20.62	4.80 | 4.93
Ribdeck gauge [mm]	1.2		20.00 | 21.60	UB 254X102X25	2.35	9.05 | 9.25	0.0135 | 0.0092	22.82 | 28.01	19.71 | 20.09	4.14 | 4.45
Slab Width [m]	3		30.00 | 35.67	UB 254X102X25	2.35	8.68 | 8.96	0.0468 | 0.0323	10.77 | 13.22	17.25 | 18.24	2.72 | 3.20
Slab Height [m]	0.12		40.00 | 42.70	UB 305X102X25	2.35	9.24 | 9.58	0.0679 | 0.0491	8.77 | 10.06	14.12 | 15.13	1.65 | 1.96
MATERIALS		6	50.00 | 56.76	UB 305X102X28	2.41	9.28 | 9.70	0.1164 | 0.0896	5.83 | 6.68	11.17 | 12.12	0.96 | 1.14
			60.00 | 63.73	UB 305X102X33	2.38	9.73 | 10.19	0.1402 | 0.1112	5.08 | 5.83	9.55 | 10.34	0.66 | 0.77
Concrete Type	LWC25		70.00 | 70.82	UB 305X102X33	2.38	9.40 | 9.88	0.1660 | 0.1335	4.43 | 5.08	8.97 | 9.72	0.58 | 0.68
			80.00 | 84.88	UB 305X127X37	2.35	9.20 | 9.56	0.2095 | 0.1745	3.87 | 3.87	7.85 | 8.44	0.43 | 0.50
Steel Type	S275		90.00 | 91.92	UB 305X127X37	2.35	9.00 | 9.35	0.2279 | 0.1934	3.61 | 3.61	7.59 | 8.10	0.40 | 0.46
			100.00 |100.00	UB 305X127X37	2.35	8.84 | 9.17	0.2389 | 0.2079	3.37 | 3.37	7.44 | 7.87	0.39 | 0.43

GEOMETRY		L [m]	% CLD_{ext} | % CLD_{real}	UB PROFILE	Y [-]	f_{mopt} M1-CM4 | M2-RMSE	η_{opt} M1-CM4 | M2-RMSE	g_{opt} M1-CM4 | M2-RMSE	R_{imp} M1-CM4 | M2-RMSE	R_{res} M1-CM4 | M2-RMSE
Length [m]	9	9	0.00 | 0.00	UB 406X140X39	2.24	6.30 | 6.30	0.0000 | 0.0000	-	15.99 | 15.99	6.88 | 6.87
Ribdeck Slab Type	Cofraplus 60		10.00 | 13.83	UB 406X140X39	2.24	6.28 | 6.29	0.0034 | 0.0024	59.34 | 68.02	15.80 | 15.86	6.43 | 6.56
Ribdeck gauge [mm]	1.2		20.00 | 22.83	UB 406X140X39	2.24	6.21 | 6.23	0.0128 | 0.0092	26.15 | 29.98	15.29 | 15.48	5.47 | 5.80
Slab Width [m]	3		30.00 | 31.83	UB 406X140X39	2.24	6.08 | 6.12	0.0298 | 0.0220	16.22 | 17.36	14.44 | 14.82	4.30 | 4.77
Slab Height [m]	0.12		40.00 | 40.83	UB 406X140X39	2.24	5.90 | 5.97	0.0540 | 0.0411	10.76 | 12.34	13.39 | 13.94	3.30 | 3.77
MATERIALS		9	50.00 | 54.33	UB 406X140X46	2.13	6.15 | 6.20	0.0951 | 0.0773	7.65 | 7.65	11.68 | 12.28	2.01 | 2.29
			60.00 | 63.33	UB 457X152X52	2.11	6.65 | 6.77	0.1226 | 0.1036	5.82 | 6.23	9.90 | 10.42	1.25 | 1.41
Concrete Type	LWC25		70.00 | 72.33	UB 457X152X52	2.11	6.41 | 6.54	0.1536 | 0.1312	5.08 | 5.44	9.18 | 9.68	1.06 | 1.19
			80.00 | 81.33	UB 457X152X52	2.11	6.18 | 6.33	0.1829 | 0.1580	4.43 | 4.74	8.61 | 9.09	0.93 | 1.04
Steel Type	S275		90.00 | 90.33	UB 457X152X60	2.01	6.51 | 6.55	0.2004 | 0.1769	4.14 | 3.86	7.64 | 8.01	0.73 | 0.81
			100.00 | 100.00	UB 457X152X60	2.01	6.39 | 6.42	0.2145 | 0.1936	3.86 | 3.61	7.44 | 7.74	0.69 | 0.75

GEOMETRY		L [m]	% CLD_{ext} | % CLD_{real}	UB PROFILE	Y [-]	f_{mopt} M1-CM4 | M2-RMSE	η_{opt} M1-CM4 | M2-RMSE	g_{opt} M1-CM4 | M2-RMSE	R_{imp} M1-CM4 | M2-RMSE	R_{res} M1-CM4 | M2-RMSE
Length [m]	12	12	0.00 | 0.00	UB 457X152X60	2.01	4.99 | 4.99	0.0000 | 0.0000	-	11.60 | 11.60	8.12 | 8.12
Ribdeck Slab Type	Cofraplus 60		10.00 | 10.51	UB 457X152X60	2.01	4.98 | 4.95	0.0016 | 0.0012	95.70 | 109.70	11.55 | 11.57	7.87 | 7.94
Ribdeck gauge [mm]	1.2		20.00 | 20.07	UB 457X152X60	2.01	4.93 | 4.91	0.0092 | 0.0066	34.37 | 36.80	11.32 | 11.40	6.86 | 7.17
Slab Width [m]	3		30.00 | 31.05	UB 533X165X66	2.02	5.47 | 5.45	0.0248 | 0.0202	18.59 | 18.59	10.79 | 10.93	4.44 | 4.73
Slab Height [m]	0.12		40.00 | 41.74	UB 533X165X66	2.02	5.30 | 5.31	0.0489 | 0.0401	11.53 | 12.34	10.08 | 10.33	3.36 | 3.68
MATERIALS		12	50.00 | 51.50	UB 533X165X66	2.02	5.11 | 5.12	0.0797 | 0.0656	8.77 | 8.77	9.30 | 9.64	2.56 | 2.87
			60.00 | 61.84	UB 533X165X74	1.93	5.21 | 5.23	0.1093 | 0.0921	6.68 | 6.68	8.51 | 8.87	1.89 | 2.12
Concrete Type	LWC25		70.00 | 72.15	UB 533X210X82	1.80	5.21 | 5.27	0.1348 | 0.1180	5.44 | 5.83	7.90 | 8.21	1.51 | 1.66
			80.00 | 82.34	UB 533X210X82	1.80	5.03 | 5.10	0.1659 | 0.1453	4.75 | 5.08	7.39 | 7.72	1.29 | 1.43
Steel Type	S275		90.00 | 92.51	UB 533X210X82	1.80	4.86 | 4.91	0.1924 | 0.1704	4.14 | 4.14	7.02 | 7.32	1.15 | 1.26
			100.00 | 100.00	UB 610X178X82	1.87	5.18 | 5.24	0.2042 | 0.1865	3.87 | 3.87	6.69 | 6.92	0.91 | 0.98

GEOMETRY		L [m]	% CLD_{ext} | % CLD_{real}	UB PROFILE	Y [-]	f_{mopt} M1-CM4 | M2-RMSE	η_{opt} M1-CM4 | M2-RMSE	g_{opt} M1-CM4 | M2-RMSE	R_{imp} M1-CM4 | M2-RMSE	R_{res} M1-CM4 | M2-RMSE
Length [m]	15	15	0	UB 533X210X82	1.80	4.12 | 4.12	0.0000 | 0.0000	-	8.93 | 8.93	8.10 | 8.10
Ribdeck Slab Type	Cofraplus 60		10.00 | 11.24	UB 533X210X82	1.80	4.11 | 4.08	0.0017 | 0.0014	95.70 | 102.46	8.90 | 8.91	7.84 | 7.89
Ribdeck gauge [mm]	1.2		20.00 | 22.29	UB 610X178X82	1.87	4.42 | 4.40	0.0099 | 0.0080	34.37 | 34.37	8.79 | 8.84	6.14 | 6.34
Slab Width [m]	3		30.00 | 30.57	UB 610X178X82	1.87	4.36 | 4.34	0.0221 | 0.0176	19.91 | 21.31	8.54 | 8.63	5.10 | 5.44
Slab Height [m]	0.12		40.00 | 41.61	UB 610X178X82	1.87	4.23 | 4.22	0.0464 | 0.0380	12.34 | 13.22	8.08 | 8.23	3.82 | 4.18
MATERIALS		15	50.00 | 52.65	UB 610X178X100	1.71	4.53 | 4.51	0.0729 | 0.0608	9.39 | 9.39	7.45 | 7.66	2.66 | 2.95
			60.00 | 60.94	UB 610X178X100	1.71	4.39 | 4.37	0.0974 | 0.0822	7.65 | 7.15	7.06 | 7.30	2.22 | 2.48
Concrete Type	LWC25		70.00 | 71.98	UB 610X229X113	1.55	4.44 | 4.48	0.1212 | 0.1048	5.83 | 6.24	6.59 | 6.82	1.77 | 1.96
			80.00 | 80.26	UB 610X229X113	1.55	4.31 | 4.35	0.1450 | 0.1280	5.08 | 5.44	6.28 | 6.50	1.55 | 1.70
Steel Type	S275		90.00 | 91.30	UB 610X229X113	1.55	4.17 | 4.19	0.1734 | 0.1542	4.43 | 4.43	5.95 | 6.17	1.36 | 1.48
			100	UB 610X229X125	1.48	4.35 | 4.33	0.1794 | 0.1614	4.43 | 4.14	5.77 | 5.97	1.24 | 1.34

References

[1] W. Hawkins, J. Orr, T. Ibell, P. Shepherd, A design methodology to reduce the embodied carbon of concrete buildings using thin-shell floors, Engineering Structures 207 (2020). doi:10.1016/j.engstruct.2020.110195.

[2] M. Setareh, Office floor vibrations: Evaluation and assessment, Proceedings of the Institution of Civil Engineers: Structures and Buildings 167 (2014) 187–199. doi:10.1680/stbu.11.00088.

[3] W. Hawkins, A. Peters, T. Mander, A weight off your mind: fl oor loadings and the climate emergency, The Structural Engineer 99 (2021) 18–20. doi:10.17863/CAM.35178.

[4] M. Royvaran, O. Avci, B. Davis, Analysis of floor vibration evaluation methods using a large database of floors framed with w-shaped members subjected to walking excitation, Journal of Constructional Steel Research 164 (2020). doi:10.1016/j.jcsr.2019.105764.

[5] M. Setareh, Vibration serviceability evaluation of office building floors due to human movements, Journal of Performance of Constructed Facilities 34 (2020). doi:10.1061/(asce)cf.1943-5509.0001457.

[6] M. S. Gonçalves, A. Pavic, R. L. Pimentel, Vibration serviceability assessment of office floors for realistic walking and floor layout scenarios: Literature review, 2020. doi:10.1177/1369433219888753.

[7] A. L. Smith, S. J. Hicks, P. Devine, Design of Floors for Vibration, second ed., SCI, 2009.

[8] T. M. Murray, E. E. Ungar, D. B. Davis, Facts for steel buildings, number 5: Vibration, 2018.

[9] M. S. Gonçalves, A. Pavic, Environmental impact of structural modifications in office floors to satisfy vibration service ability, volume 1, European Association for Structural Dynamics, 2020, pp. 1924–1931. doi:10.47964/1120.9156.19504.

[10] W. D. Varela, R. C. Battista, Control of vibrations induced by people walking on large span composite floor decks, Engineering Structures 33 (2011) 2485–2494. doi:10.1016/j.engstruct.2011.04.021.

[11] J. Roynon, Emboided carbon: Structural sensitivity study, 2020.

[12] T. H. Nguyen, I. Saidi, E. F. Gad, J. L. Wilson, N. Haritos, Performance of distributed multiple viscoelastic tuned mass dampers for floor vibration applications, Advances in Structural Engineering 15 (2012) 547–562. doi:10.1260/1369-4332.15.3.547.

[13] J. M. Soria, I. M. Díaz, J. H. García-Palacios, Further steps towards the tuning of inertial controllers for broadband-frequency-varying structures, Structural Control and Health Monitoring 27 (2020). doi:10.1002/stc.2461.

[14] X. Wang, E. Pereira, J. H. García-Palacios, I. M. Díaz, A general vibration control methodology for human-induced vibrations, Structural Control and Health Monitoring 26 (2019). doi:10.1002/stc.2406.

[15] C. Gallegos-Calderón, C. M. Renedo, M. D. G. Pulido, I. M. Díaz, A frequency-domain procedure to design tmds for lively pedestrian structures considering human–structure interaction, Structures 43 (2022) 1187–1199. doi:10.1016/j.istruc.2022.07.032.

[16] D. I. Jones, Handbook of viscoelastic vibration damping, John Wiley Sons, 2001.

[17] A. M. Baz, Active and Passive Vibration Damping, 2019. doi:10.1002/9781118537619.

[18] M. Melero, A. J. Nieto, A. L. Morales, E. Palomares, J. M. Chicharro, C. Ramiro, P. Pintado, Experimental analysis of constrained layer damping structures for vibration isolation in lightweight railway vehicles, Applied Sciences (Switzerland) 12 (2022). doi:10.3390/app12168220.

[19] C. M. C. Renedo, W. P. Ortega, I. M. Díaz, J. H. G. Palacios, Composite floor beams with constrained layer damping: Experimental tests on reduced scale models., Universidad de Oviedo, 2021, pp. 159–168.

[20] F. C. Nelson, The use of visco-elastic material to dampen vibrations in buildings and large structures, American Institute of Steel Construction Engineering Journal 5 (1968) 72–78.

[21] A. Farah, I. M. Ibrahim, R. Green, Canadian journal of revue canadienne civil bngineering de genie civil, Canadian Journal of Civil Engineering 4 (1977) 405–4011.

[22] A. Ebrahimpour, Chapter 18, externally bonded frp composite and viscoelastic materials for mitigating vibrations of floor systems, 2013. doi:10.1201/b15806.

[23] H. Ahmadi, I. Goodchild, K. Fuller, G. Canisius, A. Bougard, B. Ellis, Modelling dynamic behaviour of constrained layer damped floors usign finite element analysis, IRCO, 2002, pp. 583–595. doi:10.1515/9783110924176.v.

[24] M. Willford, P. Young, W. H. Algaard, A constrained layer damping system for composite floors, Structural Engineer 84 (2006) 31–38.

[25] A. Fischer, R. Harrison, M. Nelson, F. Lancelot, J. Hargreaves, Assessment and control of structural vibration in gyms and sports facilities, 2020, pp. 61–74.

[26] R. A. DiTaranto, Theory of vibratory bending for elastic and viscoelastic layered finite-length beams, Journal of Applied Mechanics (1965) 881–886.

[27] D. Ross, E. E. Ungar, E. M. Kerwin, Damping of plate flexural vibrations by means of viscoelastic laminae, Structural Damping,Section III, ASME (1959) 49–87.

[28] D. K. Rao, Frequency and loss factors of sandwich beams under various boundary conditions., J Mech Eng Sci 20 (1978) 271–282.

[29] S. Zegers, Lightweight floor system for vibration comfort, 2011. doi:10.6100/IR721246.

[30] J. Antar, Modelling floors with a constrained damping layer, 2011.

[31] Heathcote Industrial Polymers, Desing properties of HIP2 polymer, 2015.

[32] B. C. Chakraborty, D. Ratna, Polymers for vibration damping applications, Elsevier, 2020.

[33] E. El-Dardiry, T. Ji, Modelling of the dynamic behaviour of profiled composite floors, Engineering Structures 28 (2006) 567–579. doi:10.1016/j.engstruct.2005.09.012.

[34] C. D. Johnson, D. A. Kienholz, Finite element prediction of damping in structures with constrained viscoelastic layers, AIAA Journal 20 (1982) 1284–1290. doi:10.2514/3.51190.

[35] J. A. Rongong, Reducing vibration levels using 'smart joint' concepts, Noise and Vibration Engineering, 2000, pp. 817–824.

[36] P. J. Torvik, B. Runyon, Modifications to the method of modal strain energy for improved estimates of loss factors for damped structures, Shock and Vibration 14 (2007) 339–353.

[37] D. R. Morgenthaler, The absolute value modal strain energy method, 1991, pp. FDB1–FDB16.

[38] E. C. for Standarization, CEN (2004). Eurocode 4: Design of composite steel and concrete structures-Part 1-1: General rules and rules for buildings (EN 1994-1-1), 2004.

[39] T. M. Murray, D. E. Allen, E. E. Ungar, D. B. Davis, AISC Steel Design Guide 11. Vibrations of Steel-Framed Structural Systems Due to Human Activity, second ed., AISC, 2016.

[40] Z. O. Muhammad, P. Reynolds, Vibration serviceability of building floors: Performance evaluation of contemporary design guidelines, Journal of Performance of Constructed Facilities 33 (2019) 1–17. doi:10.1061/(ASCE)CF.1943-5509.0001280.

[41] M. R. Willford, P. Young, A Design Guide for Footfall Induced Vibration of Structures, first ed., The Concrete Society, 2006.